NASA TN D-1231

TECHNICAL NOTE

D-1231

A RIGIDLY FORCED OSCILLATION SYSTEM FOR MEASURING DYNAMIC-STABILITY PARAMETERS IN TRANSONIC AND SUPERSONIC WIND TUNNELS

By Albert L. Braslow, Harleth G. Wiley, and Cullen Q. Lee

Langley Research Center
Langley Air Force Base, Va.

NATIONAL AERONAUTICS AND SPACE ADMINISTRATION
WASHINGTON
March 1962

NATIONAL AERONAUTICS AND SPACE ADMINISTRATION

TECHNICAL NOTE D-1231

A RIGIDLY FORCED OSCILLATION SYSTEM FOR MEASURING DYNAMIC-STABILITY PARAMETERS IN TRANSONIC AND SUPERSONIC WIND TUNNELS[1]

By Albert L. Braslow, Harleth G. Wiley, and Cullen Q. Lee

SUMMARY

The mechanical and electrical details of a sting-mounted, rigidly forced, single-degree-of-freedom, oscillating yaw mechanism is described. The equipment was designed for use in transonic and supersonic wind tunnels. Dynamic-stability parameters measured with the equipment are uninfluenced by airstream turbulence or buffeting. Aerodynamically unstable bodies do not cause the mechanism to diverge, and configurations with negative damping can be tested. The accuracy of the system was investigated by application of known eddy-current damping moments.

Typical wind-tunnel results are presented for the damping in yaw and oscillatory directional stability of a simplified airplane model with 45° sweptback wing and vertical tail at transonic speeds.

INTRODUCTION

Design of guidance and control systems for aerodynamic configurations intended for flight in an atmosphere requires knowledge of the various dynamic-stability derivatives through wide ranges of flight speed. Theories have been developed which adequately describe these derivatives for configurations over which the aerodynamic flow characteristics are predictable. Local flow-separation effects often define the important dynamic parameters, however, and because of the nonlinear nature of separated flows, the effects cannot be described adequately by existing theory. The dynamic-stability characteristics must then be measured experimentally in wind tunnels.

---

[1]Supersedes declassified NACA Research Memorandum L58A28 by Albert L. Braslow, Harleth G. Wiley, and Cullen Q. Lee, 1958.

Equipment has been available for measuring dynamic-stability parameters in low-speed wind tunnels for some years (for example, see refs. 1 to 3). Because of space limitations and the effects on the measured parameters of extraneous energy sources such as airstream turbulence and buffeting, such equipment is not easily developed for use in transonic and supersonic tunnels.

Three techniques of measuring the dynamic stability of models in wind tunnels are presently available. The first technique involves the measurement of the decaying free oscillations of a model mounted on a suitable elastic restraint with a single degree of freedom. (For example, see refs. 4 and 5.) The second technique is that of self-excitation, in which a model is driven through a spring and the amplitude of oscillation is controlled by a feedback loop. (For example, see ref. 6.) Dynamic stability is determined by measuring the force required to maintain the stabilized oscillation. In the third technique, termed the inexorable method, the model is rigidly forced to oscillate at fixed amplitude and frequency while measurements are made of the force required to sustain the motion. For example, this technique was used for low-speed, low-frequency tests and is reported in reference 1.

A mechanism for accurately measuring dynamic stability at transonic or supersonic speeds must meet several stringent design requirements which generally are not so severe at low speeds. Foremost is the problem of accurately separating the relatively small aerodynamic forces which are due to the model motion from the large forces imposed on the system by inertia effects and static aerodynamic loads. The inertia loads are usually large compared with those at low speeds because of the need to oscillate at high frequencies in order to maintain realistic values of reduced frequency. Secondly, the measured dynamic stability must not be influenced by extraneous energy sources, such as airstream turbulence and buffeting. Reference 4, for example, shows how airstream turbulence can influence the model motion and, therefore, the measured dynamic stability of a configuration performing free oscillations. Thirdly, the models must be sting-mounted to minimize model-support interference. All primary mechanical and electrical equipment required to operate the model, therefore, must be enclosed in the limited space available in the model and sting support. Because of these space limitations and the large aerodynamic loads imposed, the design and arrangement of the mechanical and electrical components are quite critical.

An inexorable or rigidly forced system to measure accurately the dynamic-stability parameters in transonic and supersonic wind tunnels has been developed at the Langley Research Center of the National Aeronautics and Space Administration. The system well fulfills the foregoing requirements for measuring the dynamic stability of a model

at transonic and supersonic speeds. The system is adapted for use with mechanical or hydraulic actuation and in its present form can be used to provide single-degree-of-freedom yawing or pitching oscillations.

This paper presents the basic principles of the system and describes the pertinent electrical and mechanical relationships. As an illustration of the electrical and mechanical equipment required, a detailed description of a hydraulically driven, single-degree-of-freedom yawing mechanism is given. Typical measurements of the transonic damping in yaw and oscillatory directional-stability parameters of a simplified airplane model with 45° sweptback wing and vertical tail are presented. The model was oscillated approximately ±1° about the vertical body axis at the quarter chord of the wing mean aerodynamic chord at reduced frequencies from 0.030 to 0.057. Tests were made at angles of attack from 0° to 12.5° at Mach numbers from 0.78 to 1.30.

SYMBOLS

All aerodynamic coefficients are presented in the body system of axes and all moments are referred to the vertical oscillation axis (Z-axis), which is in the plane of symmetry at the quarter chord of the mean aerodynamic chord.

A calibration constant for moment or displacement, μamp/in-lb or μamp/radian

a maximum transformation ratio of resolver

B calibration constant, volts/in-lb

b wing span

C system damping, $\frac{\text{in-lb}}{\text{radian/sec}}$

C_n yawing-moment coefficient, M_Z/qSb

$$C_{n_r} = \frac{\partial C_n}{\partial \frac{rb}{2V}}$$

$$C_{n_{\dot{r}}} = \frac{\partial C_n}{\partial \frac{\dot{r}b^2}{4V^2}}$$

$C_{n_\beta} = \frac{\partial C_n}{\partial \beta}$

$C_{n_{\dot{\beta}}} = \frac{\partial C_n}{\partial \frac{\dot{\beta} b}{2V}}$

c	wing chord
$\bar{c}$	wing mean aerodynamic chord
e	base of natural system of logarithms
f	oscillation frequency, cycles/sec
I_Z	moment of inertia about Z-axis, slug-ft^2
i	instantaneous value of current, μamp
$\bar{i}$	average value of current, μamp
$j = \sqrt{-1}$	
K	system spring constant, in-lb/radian
k	reduced-frequency parameter referred to semispan of wing, $\omega b/2V$
M	applied moment, in-lb
M_Z	yawing moment
n	an integer (1, 2, 3, . . .)
p_t	tunnel total pressure
q	dynamic pressure, $\frac{1}{2} \rho V^2$
R	Reynolds number based on $\bar{c}$
r	angular velocity in yaw, $\frac{\partial \psi}{\partial t}$, radians/sec

$\dot{r}$	yawing acceleration, $\frac{\partial^2 \psi}{\partial t^2}$, radians/sec^2
S	wing area
t	time, sec
V	free-stream velocity
v	instantaneous voltage applied to resolver
α	angle of attack, deg
β	angle of sideslip (measured to plane of symmetry and in plane of relative wind), radians
$\dot{\beta} = \frac{\partial \beta}{\partial t}$	
γ	phase angle between model axis and resolver axis, radians
δ	phase angle between angular displacement and resolver axis, radians
θ	phase angle between applied moment and angular displacement, radians
λ	phase angle between applied moment and resolver axis, radians
ρ	mass density of air
Ψ	maximum amplitude of yaw angle, radians
ψ	instantaneous yaw angle, radians
ω	angular frequency of oscillation, radians/sec
ω_c	carrier frequency, radians/sec

Subscripts:

1	fundamental component or fundamental frequency
aero	aerodynamic characteristics
j	imaginary component

M	moment
n	the nth component
o	constant component
r	real component
ψ	displacement

BASIC PRINCIPLES

In the force-driven method of measuring dynamic stability, the model is rigidly forced to perform a single-degree-of-freedom oscillation while measurements are made of the model motion and of the moment required to sustain the motion. The model, when sinusoidally oscillating in yaw only, can be likened to a simple single-degree-of-freedom mechanical system whose characteristics can be related by the differential equation

$$I_Z\ddot{\psi} + C\dot{\psi} + K\psi = Me^{j\omega t} \tag{1}$$

A solution to this equation is

$$\psi = \Psi e^{j(\omega t-\theta)} \tag{2}$$

$$\dot{\psi} = j\omega\Psi e^{j(\omega t-\theta)} \tag{3}$$

$$\ddot{\psi} = -\omega^2\Psi e^{j(\omega t-\theta)} \tag{4}$$

Substitution of equations (2), (3), and (4) into equation (1) gives

$$\left(-I_Z\omega^2 + jC\omega + K\right)\Psi = Me^{j\theta} = M\cos\theta + jM\sin\theta \tag{5}$$

A vector diagram of equation (5) is shown in the following sketch:

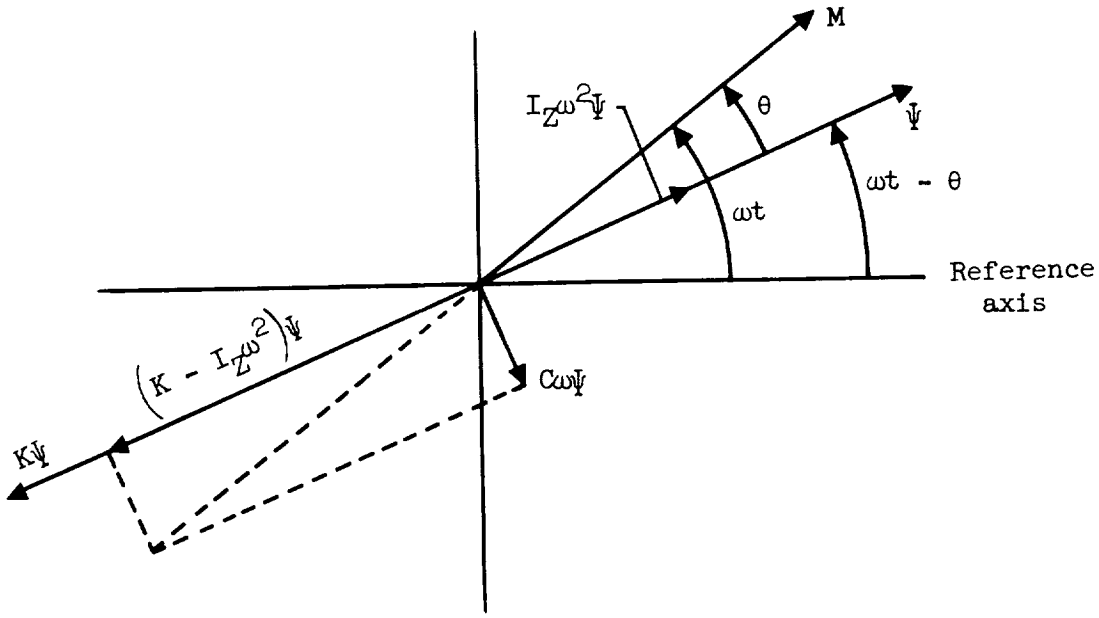

Sketch 1

In the axis system defined by the displacement, the imaginary components may be equated to give

$$C\omega\Psi = M \sin \theta$$

and the total system damping is

$$C = \frac{M \sin \theta}{\omega\Psi} \tag{6}$$

Similarly, the real components may be equated to give

$$K\Psi - I_Z\omega^2\Psi = M \cos \theta$$

and the total system spring-inertia characteristic is

$$K - I_Z\omega^2 = \frac{M \cos \theta}{\Psi} \tag{7}$$

Thus, if measurements are made of the applied moment M, the displacement ψ, the phase angle θ between M and ψ, and the angular velocity ω, the total system damping and spring characteristic can be computed.

OSCILLATING APPARATUS AND MODEL

The mechanism developed for these tests consisted of a sting-mounted model which was hydraulically forced to perform a single-degree-of-freedom angular oscillation about its vertical axis (figs. 1 and 2). Photographs of the model, mechanism, and instrumentation are shown as figures 3, 4, and 5.

The hydraulic model-oscillating system was driven by an externally mounted variable-speed, 1/2-horsepower, compound-wound, direct-current electric motor (figs. 2 and 4). Direct current was supplied to the motor by an alternating-current—direct-current motor generator set. Since accurate motor-speed control was mandatory for maximum accuracy of the data, a constant motor speed was maintained by a self-compensating circuit which regulated generator output to the motor as a function of the pump drive-motor speed.

Oscillating hydraulic pressure was supplied to the model drive piston by a hydraulic pump driven by the drive motor (figs. 2 and 4). The pump comprised a simple cam and piston and was connected to the model drive cylinder and piston by a single hydraulic line which passed through the model support sting (figs. 1 and 2). The hydraulic line was of thick-walled stainless-steel tubing. The tubing was of minimum practical length and inside diameter to minimize loss in fluid volume due to compression. (The tubing used for these tests had a 1/16-inch inside diameter and was 17 feet long. Tubing with a smaller inside diameter caused unacceptable line losses due to viscous effects for these tests.) All tubing joints and connections were smooth and fair to minimize fluid friction losses. The model drive piston was located in a cylinder in the support sting rearward of the model center of rotation and oscillated the model about the yaw pivot.

A coil spring was mounted opposite the drive piston between the model and the sting to return the model on the suction stroke of the hydraulic-pump cycle. The mean value of internal hydraulic pressure was balanced by precompression of the coil spring and the model could be symmetrically centered about the sting center line by adjustment of the coil-spring tension (figs. 1 and 2).

A constant internal hydraulic pressure, independent of the oscillating pressure applied by the pump, was maintained on the hydraulic

system by a pressure piston, lever arm, and differential weight (figs. 2 and 4). The constant-pressure system served to make up any loss of hydraulic fluid due to leakage past the "O" ring seals of the pump, model drive, and constant-pressure pistons. The mass of the constant-pressure-system assembly was much greater than the mass of the model so that essentially only the model responded to oscillations of the hydraulic fluid.

The amplitude of the model oscillation was controlled by adjustment of the hydraulic-pump cam eccentric or stroke, and was limited to a maximum of about 1° by the available gap between the fuselage shell at the base and the support sting.

As mentioned previously, a coil spring was installed between the model and the sting to return the model on the suction stroke of the hydraulic-pump cycle (figs. 1 to 3). The spring stiffness dictated the resonant frequency of the model. Since maximum accuracy of the data resulted when the model was oscillated at its natural frequency, springs with various degrees of stiffness were provided to permit a range of oscillation frequencies. (These springs will be referred to as springs 1, 2, and 3.) Coil springs were used in this investigation because of the lack of available space in the model, even though the free ends of the coil springs contributed materially to the internal mechanical or tare damping. The amount of damping contributed by the free-end condition of the springs varied with the amount of precompression in the spring, and thus considerable scatter occurred in the final data.

Design of the model flexure pivot involved several important requirements. It was necessary that the pivot permit yawing motion and still withstand the normal force, chord force, side force, pitching moments, and rolling moments imposed at angles of attack up to $12\frac{1^{\circ}}{2}$ and dynamic pressures up to about 2,000 pounds per square foot. It was necessary that the pivot contribute minimum mechanical damping in order to reduce the wind-off or tare damping. The spring stiffness of the pivot had to be small so that the greater part of the total spring stiffness of the model would be contributed by the interchangeable frequency springs, and, thus, a greater range of frequency control would be afforded. In addition, the pivot was required to have a high resistance to fatigue failure. After considerable experimentation, a successful fabrication technique for the flexure pivot was evolved. The pivot comprised a cruciform arrangement of four 0.007-inch-thick flat beryllium-copper leaves installed radially in a hardened steel center post as shown in the following sketch:

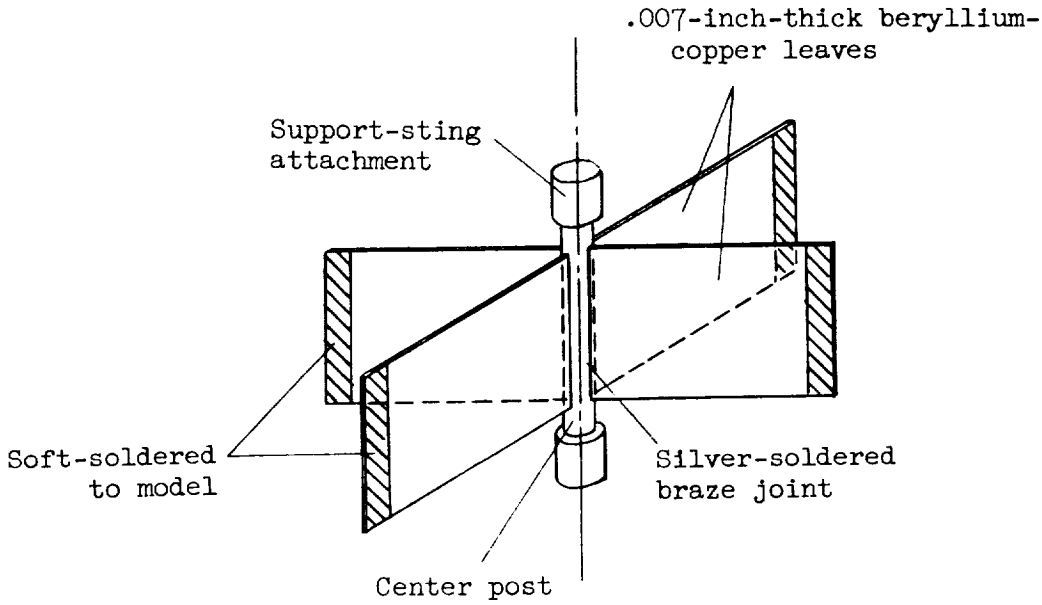

Sketch 2

The flexure pivot was assembled and the leaves brazed in the center post with powdered silver solder and cadmium. After the brazing operation, the beryllium-copper leaves were tempered to provide maximum strength and resistance to fatigue. The flexure-pivot assembly was then installed in the model with soft solder (figs. 1 to 3).

The model was forced to oscillate by the model piston, which drove the model through a moment beam equipped with a strain gage (figs. 1 to 3). The moment beam was made of aluminum and was designed to provide maximum strain or gage response for minimum total deflection. Thus, the rigid-forcing requirement for this technique was met. The moment beam was driven by the piston through a ball-and-socket joint so that strain applied to the gage beam was the result of a directly applied yawing moment only. The arrangement was of such a nature that the measured value of damping moment was independent of any normal force, rolling moment, or pitching moment applied to the model. It is pertinent to point out that the moment strain gage, when located at the model, is subjected only to those forces applied to the oscillating model. Thus for this mechanism, although the free ends of the coil spring result in measurable mechanical friction as described previously, the friction in the ball-and-socket joint and components of the hydraulic-drive system do not affect the measured results.

The model sting was designed to have a high natural frequency so that the somewhat lower values of model oscillation frequency would not excite motion of the sting. The model and sting were coupled only through the weak yaw flexure pivot and no appreciable sting motion resulted.

In operation of the system, calibrated outputs of moment and displacement alternating-current strain gages are passed through coupled electrical sine-cosine resolvers which rotate at the frequency of oscillation (figs. 2, 3, and 4). The resolvers transform the moment and amplitude functions into orthogonal components which are demodulated and simultaneously measured on direct-current microammeters (fig. 5). From these components the applied moment and displacement and the phase angle between them can be found, and with the known oscillation frequency the aerodynamic-damping and oscillatory-directional-stability moments can be computed.

A two-view drawing of the model tested is presented in figure 6. The model had a steel wing with 45° sweepback at the quarter-chord line, an aspect ratio of 4.0, a taper ratio of 0.3, and an NACA 65A006 airfoil section parallel to the stream. The wing was mounted on the fuselage center line and had no dihedral or twist. The vertical tail was made of brass and had 45° sweepback at the quarter-chord line, an aspect ratio of 2.0, a taper ratio of 0.3, and an NACA 65A006 airfoil parallel to the stream. No horizontal tail was used. The fuselage was a simple body of revolution with a fineness ratio of 7. The removable nose was made of aluminum and the rest of the fuselage was made of phosphor bronze with a removable upper section (fig. 3). The center of gravity of the model was coincident with the vertical axis of rotation, which was in the plane of symmetry at the quarter chord of the mean aerodynamic chord.

The model and oscillating apparatus were mounted on a sting support mechanism which permitted testing at angles of attack up to $12\frac{1}{2}^{\circ}$ while maintaining the model approximately on the wind-tunnel center line. A fouling-light circuit was arranged to indicate contact between the model base and sting (fig. 5), and tests were not made when such contact existed.

ELECTRICAL RELATIONS AND DATA REDUCTION

A block diagram of the electronic circuit used to measure the applied moment is shown in figure 7. A similar circuit was used to measure the angular displacement.

The oscillator supplies a 10-volt, 3-kilocycle carrier voltage to the moment strain-gage bridge circuit. After the bridge has been balanced, any moment applied to the model unbalances the bridge and gives an output voltage directly proportional to the applied moment. When the moment is oscillatory, the resulting output signal is a modulated 3-kilocycle voltage whose modulation frequency is that of the applied

moment or model oscillation frequency. The signal is then amplified by the linear amplifier and passed through a resolver which resolves the signal into two orthogonal components. (See refs. 2 and 7.) The reference component, or the part of the signal that is in phase with the resolver rotor, is called the real component. The quadrature component, or the part of the signal that is 90° out of phase with the resolver rotor, is called the imaginary component. The resolver is essentially a transformer with a single fixed primary winding and two secondary windings wound at right angles to each other on a rotor. The flux linkage of the rotor windings and, hence, the transformation ratio is proportional to the sine of the angle that the windings make with the flux produced by the primary winding current. Since the secondary windings are oriented 90° apart, the primary winding current when passed through the resolver is multiplied by $(a \sin \omega_1 t)$ in one secondary winding and by $(a \cos \omega_1 t)$ in the other secondary winding. The individual outputs are then demodulated to remove the 3-kilocycle carrier frequency from the signal. The resulting output currents are read on direct-current microammeters of sufficient time constant to yield the average value of each component.

The resolver, when rotated at the fundamental model frequency ω_1, plays an important part in the ability of the system to measure only the moment required to overcome the system damping even in the presence of random energy inputs such as those due to airstream turbulence and buffeting. The forcing function, or applied moment, under these conditions is nonsinusoidal and may be expressed by the Fourier series

$$M = M_o + \sum_{n=1}^{\infty} M_n \sin(n\omega_1 t + \lambda_n) \tag{8}$$

This forcing function occurs when there are an initial unbalance of the bridge M_o and harmonics due to the influence of stream turbulence or buffeting. The voltage applied to the resolver is then

$$\begin{aligned} v_M &= BM \sin \omega_c t \\ &= BM_o \sin \omega_c t + B \sin \omega_c t \sum_{n=1}^{\infty} M_n \sin(n\omega_1 t + \lambda_n) \end{aligned} \tag{9}$$

Since the resolver is coupled to the model drive system and is driven at the fundamental frequency of the model, the demodulated output current for the real component is given by

$$i_{M_r} = A_{M_r} M_o \sin \omega_1 t + A_{M_r} \sin \omega_1 t \sum_{n=1}^{\infty} M_n \sin(n\omega_1 t + \lambda_n) \qquad (10)$$

The average value of the output current may be obtained by integrating equation (10) over a long period of time τ, which is the process actually performed by the damped microammeters as shown in the following development.

The first term of equation (10) can be produced by a static unbalance of the bridge, and its average or integrated value is

$$\bar{i}_{M_r,o} = \lim_{\tau \to \infty} \frac{A_{M_r} M_o}{\omega_1 \tau}(1 - \cos \omega_1 \tau) = 0 \qquad (11)$$

Thus, any static unbalance of the bridge integrates to zero.

The average or integrated value of the second term of equation (10), which includes the fundamental and all higher harmonics of the applied moment, is for $n = 1$

$$\bar{i}_{M_r,1} = \frac{A_{M_r} M_1}{2} \cos \lambda_1 \qquad (12)$$

and for $n \neq 1$

$$\bar{i}_{M_r,n} = \lim_{\tau \to \infty} \frac{A_{M_r} M_n}{2\omega_1 \tau} \left\{ \left[\frac{\sin(n-1)\omega_1 \tau}{n-1} - \frac{\sin(n+1)\omega_1 \tau}{n+1} \right] \cos \lambda_n + \left[\frac{\cos(n-1)\omega_1 \tau}{n-1} - \frac{\cos(n+1)\omega_1 \tau}{n+1} - \frac{2}{n^2-1} \right] \sin \lambda_n \right\}$$

$$= 0 \qquad (13)$$

Thus, all random noise in the signal, at frequencies other than the fundamental, which may be produced by tunnel turbulence or buffeting is integrated to zero (eq. 13). Equation (12) includes only the average value of the real component of output current produced by the applied moment at the fundamental frequency of the resolvers (n = 1). The fundamental component of moment will contain a measure of any tunnel turbulence or buffeting energy which occurs at the frequency of oscillation (n = 1); but since the input from turbulence and buffeting is random and the total energy involved is spread over a rather wide frequency spectrum, the energy remaining at the single discrete frequency of oscillation is infinitesimally small. Thus, the average or integrated value of moment current as measured still contains only the fundamental component of moment required to oscillate the model. The integration of the output currents is accomplished by applying the resolver output to a suitably damped microammeter. The fundamental component of moment is then indicated as a direct-current deflection of the meter needle, and static unbalance of the bridge and any unwanted harmonics in the signal appear as damped fluctuations of the meter needle which may be visually averaged with time.

Similarly, when integrated over time, the imaginary component of the moment current, which is taken from the other terminals of the resolver, is

$$\bar{i}_{M_{j,1}} = \frac{A_{M_j} M_1}{2} \sin \lambda_1 \tag{14}$$

When equation (12) is multiplied by the calibration factor $2/A_{M_r}$, the real component of the applied moment is given by

$$M_r = \frac{2\bar{i}_{M_r}}{A_{M_r}} = M_1 \cos \lambda_1 \tag{15}$$

A vector diagram of the system is given in the following sketch:

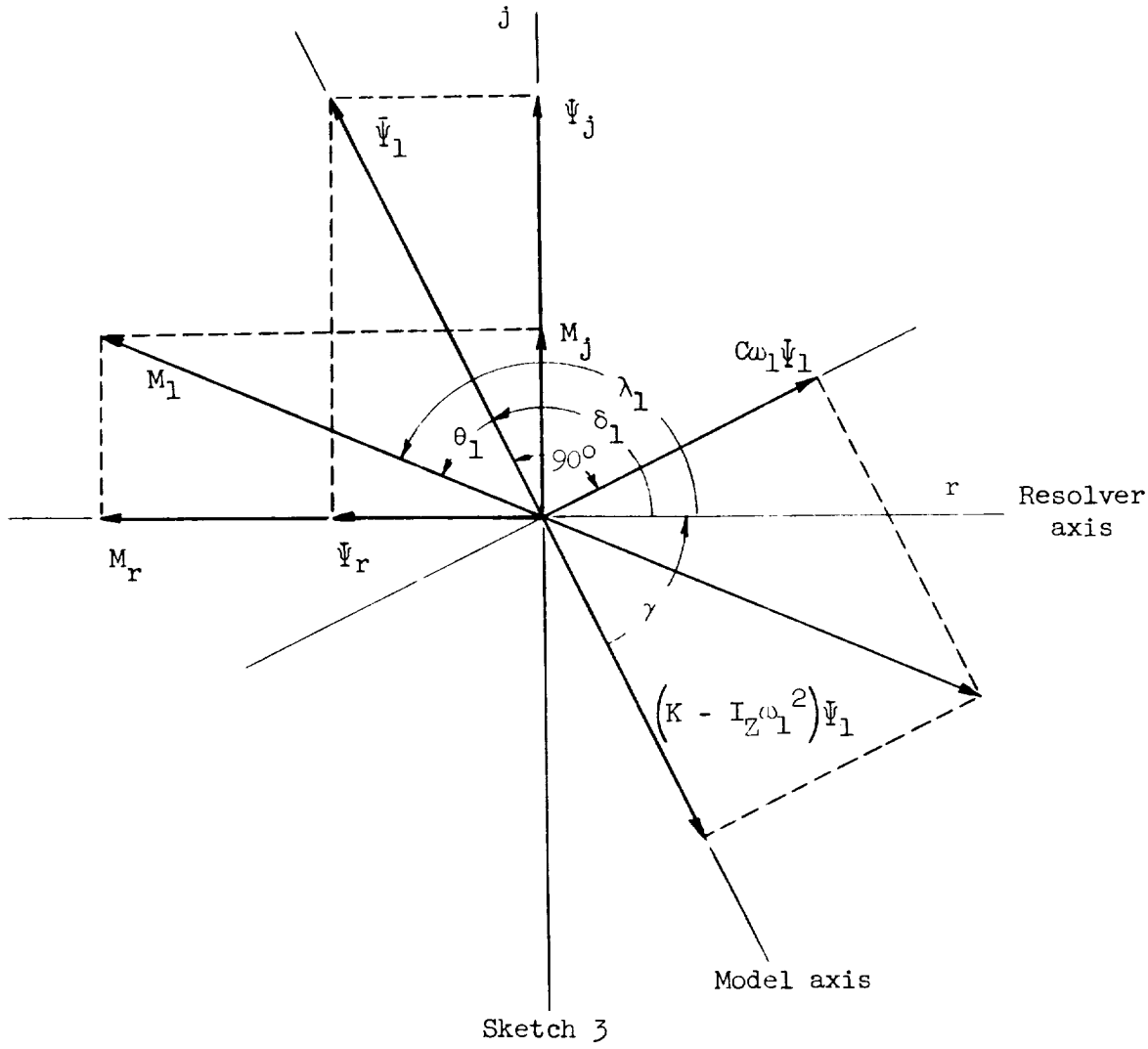

Sketch 3

When equation (14) is multiplied by $2/A_{M_j}$, the imaginary component is given by

$$M_j = \frac{2\bar{I}_{M_j}}{A_{M_j}} = M_1 \sin \lambda_1 \tag{16}$$

The fundamental of the applied moment is then

$$M_1 = \sqrt{M_r^2 + M_j^2} \tag{17}$$

and the phase angle that the fundamental component of the signal makes with the resolver rotor or reference axis (sketch 3) is given by

$$\lambda_1 = \tan^{-1} \frac{M_j}{M_r} \tag{18}$$

A calibrated voltage proportional to the angular displacement of the model was supplied by a strain gage mounted on a flexible displacement beam which was connected between the oscillating model and the rigid support sting (figs. 1 and 2). The displacement output voltage was passed through a second resolver in a manner similar to that previously described for the moment signal. The components and phase angle of the angular displacement may therefore be determined as

$$\Psi_r = \frac{2\bar{i}_{\psi_r}}{A_{\psi_r}} = \Psi \cos \delta_1 \tag{19}$$

$$\Psi_j = \frac{2\bar{i}_{\psi_j}}{A_{\psi_j}} = \Psi \sin \delta_1 \tag{20}$$

$$\Psi_1 = \sqrt{\Psi_r^2 + \Psi_j^2} \tag{21}$$

$$\delta_1 = \tan^{-1} \frac{\Psi_j}{\Psi_r} \tag{22}$$

The rotors of the moment and displacement resolvers are alined to be in phase but are set at an arbitrary angle γ with respect to the model axes (sketch 3). The angle γ includes any delay that may exist between the resolvers and the model.

From sketch 3 it is seen that the phase angle between the applied moment and angular displacement is given by

$$\theta_1 = \lambda_1 - \delta_1 = \tan^{-1} \frac{M_j}{M_r} - \tan^{-1} \frac{\Psi_j}{\Psi_r} \tag{23}$$

and any time delay or phase angle γ between the drive motor and the model is subtracted out.

Oscillograph records were made of the frequency of oscillation of the model during tests. These records were indexed by the operating circuit of the meter-recording cameras to insure that instantaneous values of oscillatory frequency f could be recorded simultaneously with the meter readings of moment and displacement. The angular velocity can then be determined as

$$\omega_1 = 2\pi f_1 \tag{24}$$

Thus, from values of moment M_1, displacement Ψ_1, phase angle θ_1, and angular velocity ω_1, the system damping can be computed as

$$C_1 = \frac{M_1 \sin \theta_1}{\Psi_1 \omega_1}$$

and the system spring-inertia constant can be computed as

$$K_1 - I_Z \omega_1^2 = \frac{M_1 \cos \theta_1}{\Psi_1}$$

Aerodynamic damping and the aerodynamic spring-inertia characteristic or oscillatory directional stability were determined by subtracting the mechanical or tare characteristics of the system from the total system characteristics measured in the wind tunnel as follows:

$$(C_1)_{aero} = \left(\frac{M_1 \sin \theta_1}{\Psi_1 \omega_1}\right)_{wind\ on} - \left(\frac{M_1 \sin \theta_1}{\Psi_1 \omega_1}\right)_{wind\ off} \tag{25}$$

$$\left(K_1 - I_Z \omega_1^2\right)_{aero} = \left(\frac{M_1 \cos \theta_1}{\Psi_1}\right)_{wind\ on} - \left(\frac{M_1 \cos \theta_1}{\Psi_1}\right)_{wind\ off} \tag{26}$$

where the wind-on and wind-off values are determined at the same oscillation frequency.

These aerodynamic characteristics were reduced to coefficient form in the manner described in reference 3 so that the damping parameter is

$$C_{n_r} - C_{n_{\dot{\beta}}} \cos \alpha = - \frac{(C_l)_{aero}(2V)}{qSb^2} \tag{27}$$

and the oscillatory-directional-stability parameter is

$$C_{n_\beta} \cos \alpha + k^2 C_{n_{\dot{r}}} = \frac{\left(K_l - I_Z \omega_l^2\right)_{aero}}{qSb} \tag{28}$$

The expression $\cos \alpha$ appears in equations (27) and (28) because the coefficients are expressed in the body-axis system.

ACCURACY

It is pertinent to point out a factor which affects accuracy of measurement. As developed previously, system damping is expressed as

$$C_l = \frac{M_l \sin \theta_l}{\Psi_l \omega_l}$$

It is obvious in sketch 3 that, as the phase angle θ_l between the moment vector M_l and the displacement vector Ψ_l approaches 90°, the variation of $\sin \theta_l$ with θ_l is small, and high precision in the measurement of θ_l is not required. Since a value of $\theta_l = 90^\circ$ corresponds to resonance (moment is in phase with velocity or 90° out of phase with displacement), for best accuracy measurements were made near the resonant condition.

Ability of the force-driven mechanism to measure damping in yaw was determined by applying a known damping moment while oscillating the model. The model wings were replaced by dummy wings of sheet copper, which oscillated between the poles of a double electromagnet (fig. 8). When the electromagnet coils were energized, eddy-current losses set up in the copper plate were proportional to the oscillatory velocity of the plate and applied a damping moment to the model. With the drive

piston removed, the damping moment applied to the model by the eddy-current damper was measured by the well-known free-decay technique for various values of current applied to the electromagnet. With the drive piston replaced, the model was forced to oscillate with similar applied eddy-current moments and the moments were measured by the technique used in this investigation. Agreement between the results of the two methods of measuring damping moments was excellent (fig. 9).

The results presented in this report include results of intentional repetition of test conditions during four separate tests. Throughout the tests, changes in technique were continually made to improve data accuracy by reducing the value of internal or tare damping (particularly the friction of the coil spring), improving flexure-pivot characteristics, increasing instrumentation response, and improving oscillation frequency control. The data presented for the four tests, therefore, contain scatter which was attendant on the continual development of the method of testing. Based on repeatability throughout the full program of the tests, the accuracy of measuring the parameter $C_{n_r} - C_{n_{\dot{\beta}}} \cos \alpha$ was about ± 0.08 and the accuracy of measuring $C_{n_\beta} \cos \alpha + k^2 C_{n_{\dot{r}}}$ was about ± 0.03. Accuracy of measuring Mach number was about ± 0.01 and of measuring angle of attack was about $\pm 0.2^\circ$.

The experimental aerodynamic tests were made in the Langley transonic blowdown tunnel, which has a slotted octagonal test section with 26 inches between flats. Tests were made through a Mach number range from about 0.78 to 1.30. Previous experience had indicated that aerodynamic characteristics of models of the present size are affected by the intersection of wall-reflected disturbances with the model in the Mach number range between about 1.04 and 1.13. No data are presented, therefore, for this Mach number range.

The tests were made at tunnel stagnation pressures of approximately 30 and 50 pounds per square inch absolute with corresponding Reynolds numbers, based on wing mean aerodynamic chord, of about 1.5×10^6 and 2.5×10^6, respectively (fig. 10). The results of reference 8 indicate that, for the Reynolds number range of the present investigation, it is extremely unlikely that the model surface condition was smooth enough to permit attainment of laminar boundary-layer flow.

Measurements were made of the damping-in-yaw parameter $C_{n_r} - C_{n_{\dot{\beta}}} \cos \alpha$ and the oscillatory directional-stability derivative $C_{n_\beta} \cos \alpha + k^2 C_{n_{\dot{r}}}$ at angles of attack of 0°, 5°, and 8° throughout most of the Mach number range for a stagnation pressure of 30 pounds per square inch absolute. Additional tests were made at $\alpha = 10^\circ$ for Mach numbers up to about 1.02 and at $\alpha = 12\frac{1}{2}^\circ$ for Mach numbers up to 0.87.

Tests at a stagnation pressure of 50 pounds per square inch absolute were restricted to angles of attack of 0° and 5° because of high lift loads on the model. The reduced-frequency parameter $\omega b/2V$ varied from 0.030 to 0.057 for the tests.

EXPERIMENTAL RESULTS

Experimental measurements of the damping-in-yaw parameter $C_{n_r} - C_{n_{\dot{\beta}}} \cos \alpha$ and the oscillatory directional stability parameter $C_{n_\beta} \cos \alpha + k^2 C_{n_{\dot{r}}}$ for a simplified airplane model with 45° sweptback wing and vertical tail, as tested on the force-driven dynamic stability mechanism described in this paper, are presented in figures 11 and 12. The reduced-frequency parameter $\omega b/2V$ for the tests is presented in figure 13.

Results of the tests show that the damping-in-yaw parameter $C_{n_r} - C_{n_{\dot{\beta}}} \cos \alpha$ was independent of angle of attack at a subsonic Mach number of 0.87 up to an angle of attack of $12\frac{1}{2}^\circ$. At Mach numbers of 0.95 and above, $C_{n_r} - C_{n_{\dot{\beta}}} \cos \alpha$ had increased markedly at an angle of attack of 5°, and further increases were evident as Mach number and angle of attack were increased. References 3 and 9 show a sharp increase in damping in yaw at angles of attack of about 14° for swept wings at low speeds; this increase was attributed to flow separation on swept wings at these angles of attack. The increase in $C_{n_r} - C_{n_{\dot{\beta}}} \cos \alpha$ for the present tests appears to occur at much lower angles of attack for high subsonic and supersonic speeds and may be attributed to shock-induced separation at the higher Mach numbers. How flow separation increases the damping in yaw is not immediately apparent, but the phenomenon may result from a time lag in the effects of separation from each wing (ref. 3). The oscillatory directional stability parameter $C_{n_\beta} + k^2 C_{n_{\dot{r}}}$ decreased with angle of attack for angles of attack above 5° for Mach numbers from 0.95 to 1.30.

DISCUSSION

The experimental aerodynamic and eddy-current damper results presented in this paper show the ability of the rigidly forced, hydraulically operated yawing mechanism to measure dynamic-stability derivatives

in a transonic wind tunnel. The scatter in the data obtained during four separate test series was associated with attempts to develop components of minimum mechanical friction and to improve testing procedures; it was not due to any fallacy in the basic principles of the method. A review of several mechanical design details which prevented, in this first mechanism, the complete fulfillment of the conditions desired will be given in order to stress the mechanical and operational problem areas and to indicate solutions that were achieved in a second mechanism described in reference 10.

Space limitations required that a coil spring with free ends be used as a tuning spring. Since the coil spring was mounted between the oscillating model and the fixed sting, the moment beam also measured the mechanical friction of the free ends of the spring. Several different coil-spring designs were used (for example, double-wound coils) in attempts to decrease the end friction, but none proved entirely satisfactory with regard to the friction magnitude. In addition, the testing procedure was considerably complicated by the fact that the hydraulic-pressure preload affected the coil-end friction; a measurement of the system friction was therefore required before each wind-tunnel test run. (It is again pertinent to note, however, that friction caused by the piston ball-and-socket joint and the other driving components which were mounted behind the moment-sensing elements (figs. 1 to 3) was not measured by the moment beam.)

A second operational problem was caused by the fabricated flexure pivot. The small, thin flexure leaves were of marginal strength and restricted the angle of attack at which tests could be made. In addition, the soft-solder attachments to the model allowed slight creep which also contributed to the mechanical friction measured by the moment beam.

The third consideration involves the single hydraulic driving piston. Before operation, the hydraulic-pressure preload on the piston was carefully balanced by adjustment of the compression load of the coil spring so that the model was alined with the sting center line. During oscillation, the increased hydraulic pressure on the single drive piston provided the driving stroke to the model and the compressed coil spring provided the return stroke. The sinusoidal oscillation of the model was thus rigidly maintained. Precise alinement of the model about the sting center line was a function of the balance of the hydraulic-pressure preload, the coil-spring force, and the external static aerodynamic moments about the model oscillation axis. For the symmetrical model oscillating about its vertical axis, as for these tests, the static aerodynamic moments were also symmetrical; therefore, alinement of the model with respect to the sting was maintained by repeated adjustments of the coil-spring compression force. This single-piston—coil-spring driving system is not easily adapted for pitching oscillations, however, as complicated

adjustments of the spring force would be necessary to balance the asymmetric pitching moments resulting from changes in angle of attack.

The basic principles of the system described herein have been incorporated in the development of a mechanically driven mechanism which is described in reference 10. This mechanically driven mechanism incorporates several important design features which eliminate the operational problems of the hydraulic mechanism. The test model is mounted on a moment-sensitive strain-gage balance arm which is positively forced to oscillate by a mechanical scotch-yoke and crank arrangement, and thus the positive sinusoidal motion required is more easily provided. The driving motor is of sufficient power and the driving linkages are of adequate strength to provide inexorable sinusoidal oscillation for all anticipated operating conditions. The model cannot become misalined with respect to the sting, and therefore pitching as well as yawing oscillations can be made at angles of attack or sideslip.

A cantilever spring is rigidly mounted to the sting and flexibly attached to the oscillating model by a thin metal flexure plate. Unlike the coil spring in the hydraulic mechanism, this cantilever tuning-spring assembly has very low mechanical friction of constant value which can be easily calibrated and subtracted from the wind-tunnel measurements.

The moment beams are mounted between the oscillating model and the pivot in the mechanically driven mechanism. With this arrangement the moments due to friction in the pivot are not measured, and so it was possible to utilize a pivot comprised of a simple shaft and needle-bearing assembly.

The mechanical and electrical principles described in this paper and in reference 10 provide a basis for the design of inexorable force-driven dynamic-stability-measuring mechanisms which are unaffected by random energy sources such as airstream turbulence or buffeting. These mechanisms are particularly suitable for use in transonic and supersonic wind tunnels. The principles can be applied to mechanisms designed for pitching, yawing, or rolling oscillations. Since the oscillations are rigidly forced, the frequency and amplitude are controlled by the operator and are not dictated by the aerodynamic characteristics of the test configuration. The system is particularly well adapted to the testing of unorthodox aerodynamic configurations whose stability is unpredictable, inasmuch as unstable bodies do not cause the mechanism to diverge and configurations with negative damping can be tested.

CONCLUSIONS

An inexorable or force-driven, hydraulically operated, single-degree-of-freedom, oscillating yawing mechanism for the measurement of dynamic-stability derivatives of aerodynamic configurations in a transonic wind tunnel has been developed and successfully used. Wind-tunnel and eddy-current-damper tests demonstrate the ability of the mechanism to measure damping moments. Comparison of the characteristics of this hydraulically operated mechanism with those of an advanced mechanically driven mechanism are made in this paper and emphasize these important design principles:

1. The forcing function should be capable of rigidly driving the model sinusoidally in the presence of large and nonlinear aerodynamic moments. The frequency and amplitude are thus controlled by the operator and are not dictated by the aerodynamic characteristics of the test configuration. Unstable bodies, therefore, do not cause the mechanism to diverge and configurations with negative damping can be tested.

2. The strain-gage beams or other moment-sensing elements should have maximum sensitivity with minimum total deflection to maintain system rigidity. The applied moments and model response should be directly measured at the model to minimize errors due to possible distortion of the driving linkages.

3. The effects of internal mechanical damping on the measured moments should be minimized by the use of flexure pivots or by location of the moment-sensing elements between the model and the first source of appreciable mechanical friction.

4. A tuning spring of low mechanical damping should be incorporated to balance out the high inertia forces resulting from operation at high frequencies.

5. The electronic equipment should allow operation in the presence of extraneous energy inputs. This requirement and the rigidly controlled model oscillation permit operation in the presence of airstream turbulence and buffeting. The equipment is thus designed for use in transonic and supersonic wind tunnels.

Langley Aeronautical Laboratory,
National Advisory Committee for Aeronautics,
Langley Field, Va., January 8, 1958.

REFERENCES

1. Queijo, M. J., Fletcher, Herman S., Marple, C. G., and Hughes, F. M.: Preliminary Measurements of the Aerodynamic Yawing Derivatives of a Triangular, a Swept, and an Unswept Wing Performing Pure Yawing Oscillations, With a Description of the Instrumentation Employed. NACA RM L55L14, 1956.

2. Bratt, J. B., Wight, K. C., and Tilly, V. J.: The Application of a "Wattmeter" Harmonic Analyser to the Measurement of Aerodynamic Damping for Pitching Oscillations. R. & M. No. 2063, British A.R.C., 1942.

3. Campbell, John P., Johnson, Joseph L., Jr., and Hewes, Donald E.: Low-Speed Study of the Effect of Frequency on the Stability Derivatives of Wings Oscillating in Yaw With Particular Reference to High Angle-of-Attack Conditions. NACA RM L55H05, 1955.

4. Cahill, Jones F., and Bird, John D.: Low-Speed Tests of a Free-To-Yaw Model in Two Wind Tunnels of Different Turbulence. NACA RM L51L14, 1952.

5. Palmer, William E.: A Wind-Tunnel Investigation of the Low-Amplitude Damping in Yaw and Directional Stability of a Fuselage-Tail Configuration at Mach Numbers Up to 1.10. NACA RM L57C15, 1957.

6. Beam, Benjamin H.: A Wind-Tunnel Test Technique for Measuring the Dynamic Rotary Stability Derivatives at Subsonic and Supersonic Speeds. NACA Rep. 1258, 1956. (Supersedes NACA TN 3347.)

7. Lessing, Henry C., Fryer, Thomas B., and Mead, Merrill H.: A System for Measuring the Dynamic Lateral Stability Derivatives in High-Speed Wind Tunnels. NACA TN 3348, 1954.

8. Braslow, Albert L., and Knox, Eugene C.: Simplified Method for Determination of Critical Height of Distributed Roughness Particles for Boundary-Layer Transition at Mach Numbers From 0 to 5. NACA TN 4363, 1958.

9. Fisher, Lewis R.: Experimental Determination of Effects of Frequency and Amplitude on the Lateral Stability Derivatives for a Delta, a Swept, and an Unswept Wing Oscillating in Yaw. NACA Rep. 1357, 1958. (Supersedes NACA RM L56A19.)

10. Bielat, Ralph P., and Wiley, Harleth G.: Dynamic Longitudinal and Directional Stability Derivatives for a 45° Sweptback-Wing Airplane Model at Transonic Speeds. NASA TM X-39, 1959.

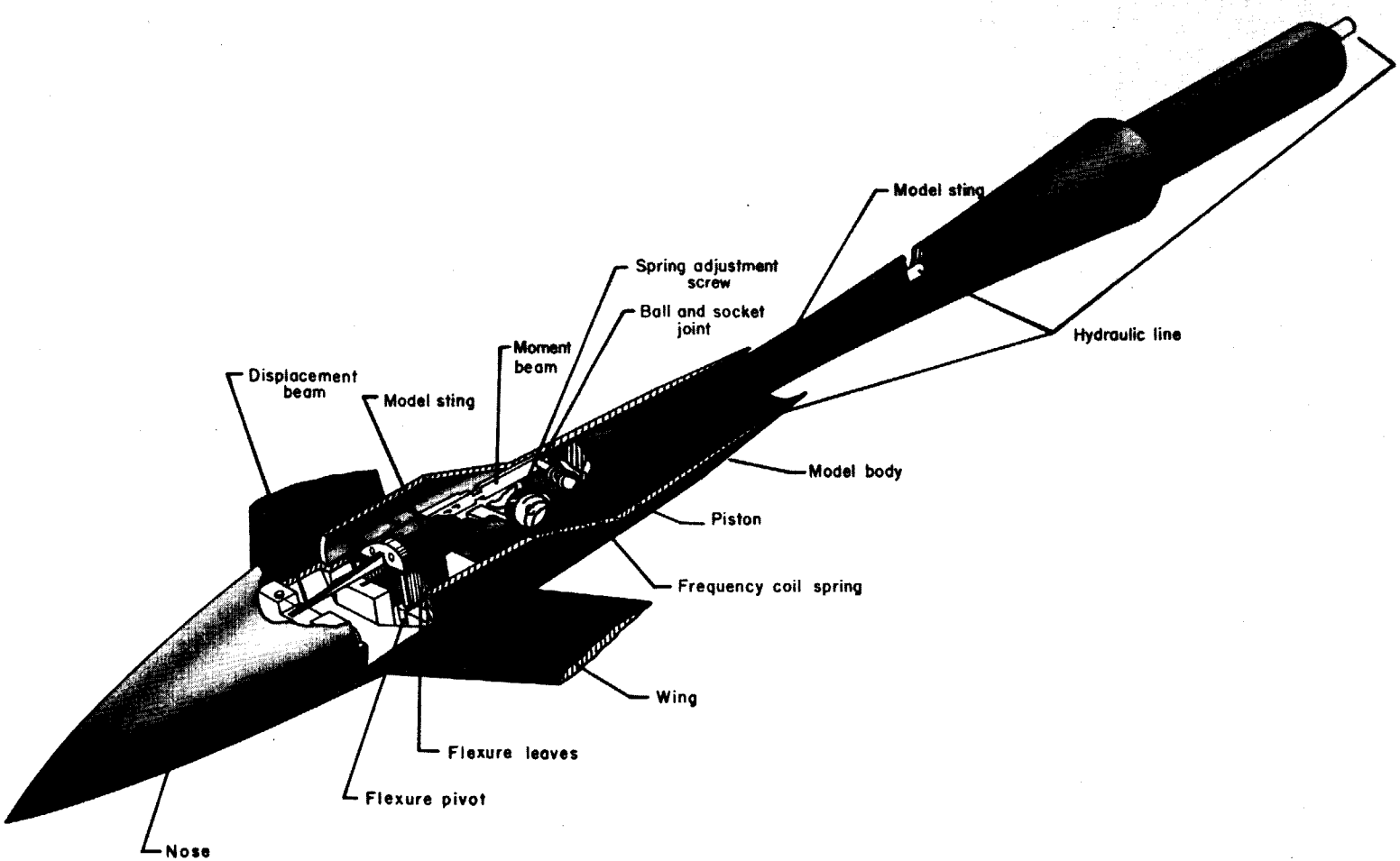

Figure 1.- Isometric sketch of model, internal mechanism, and sting support.

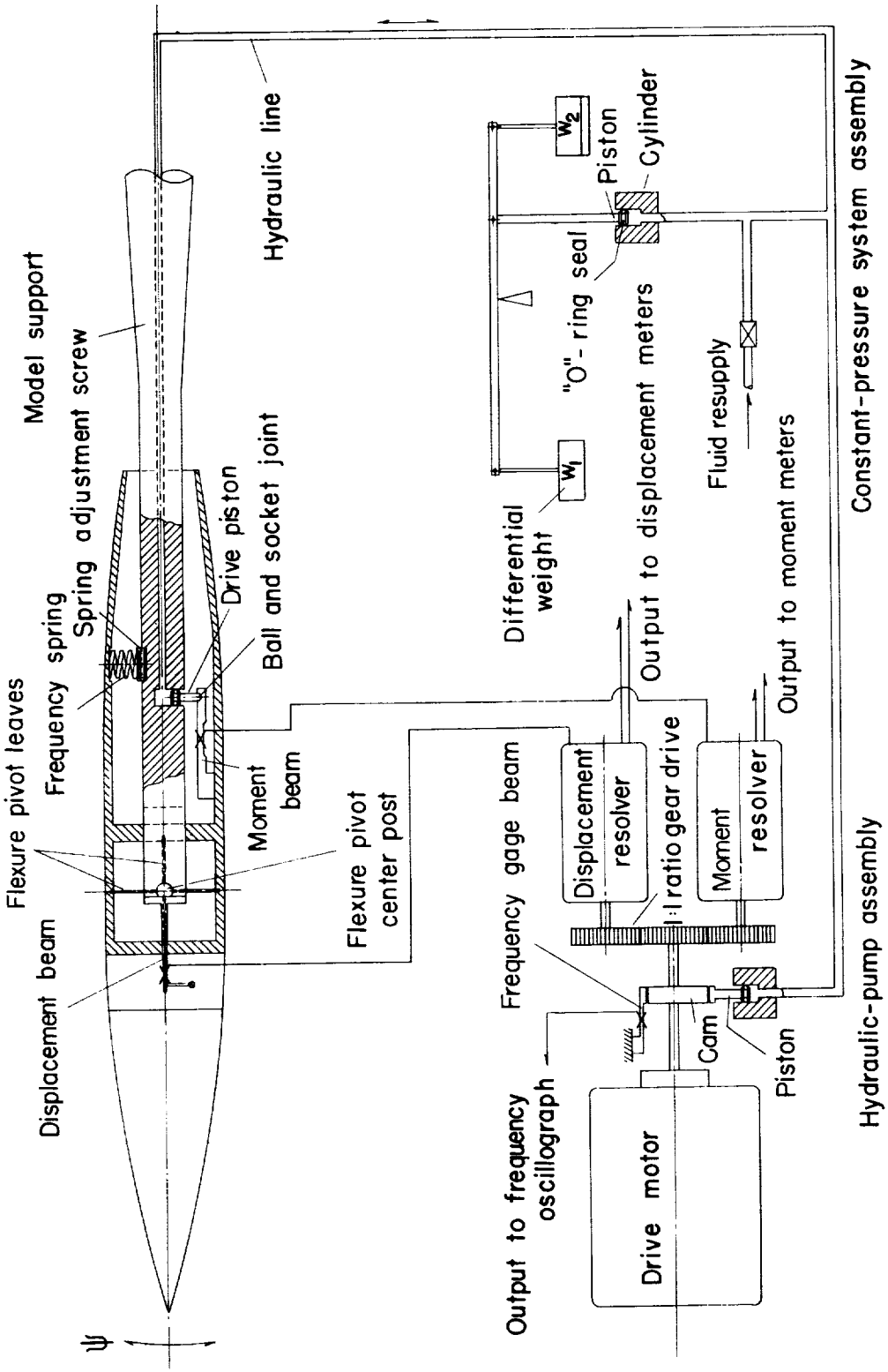

Figure 2.- Sketch of model and driving system components.

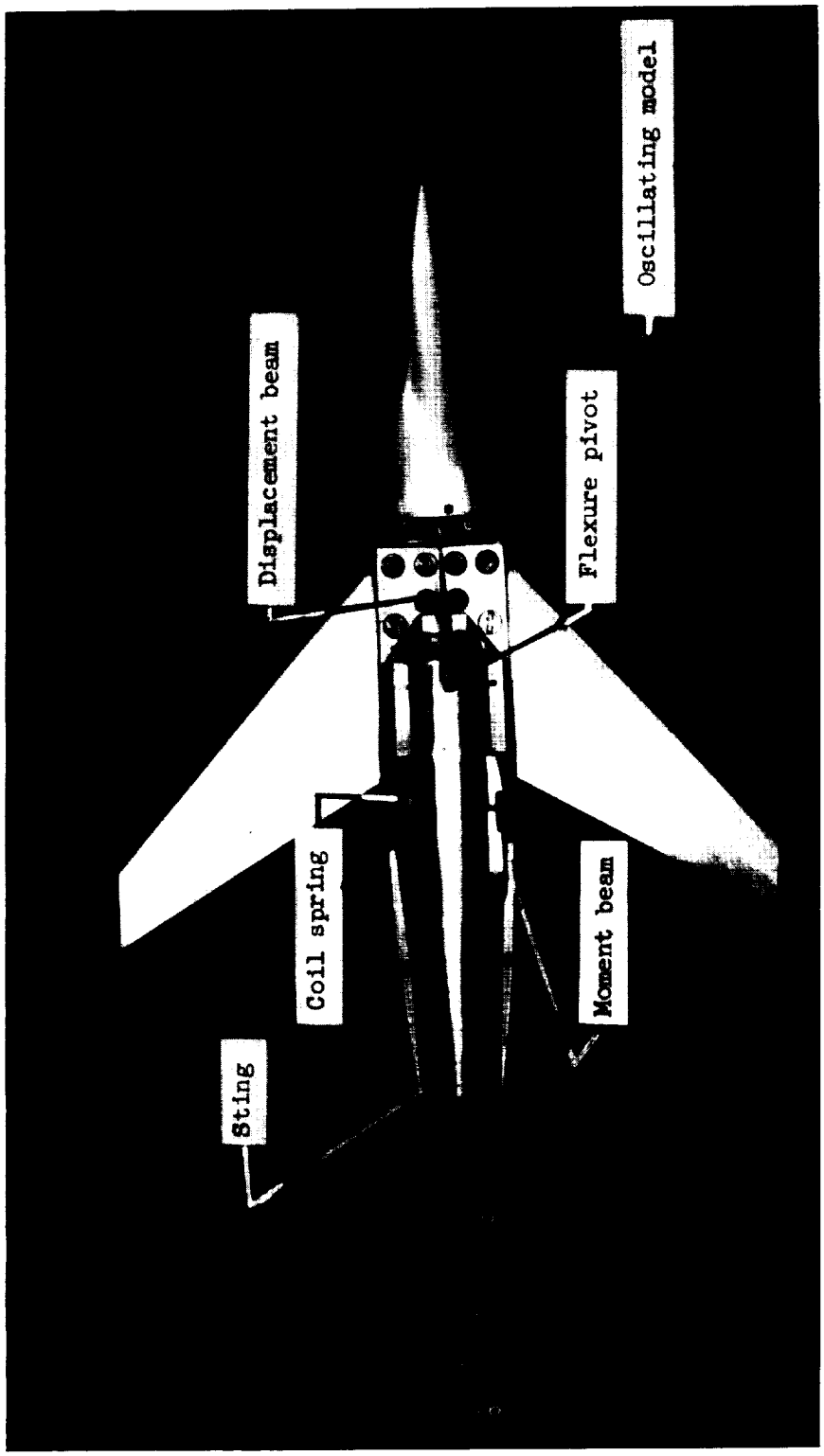

L-96055.1

Figure 3.- Model and internal mechanism.

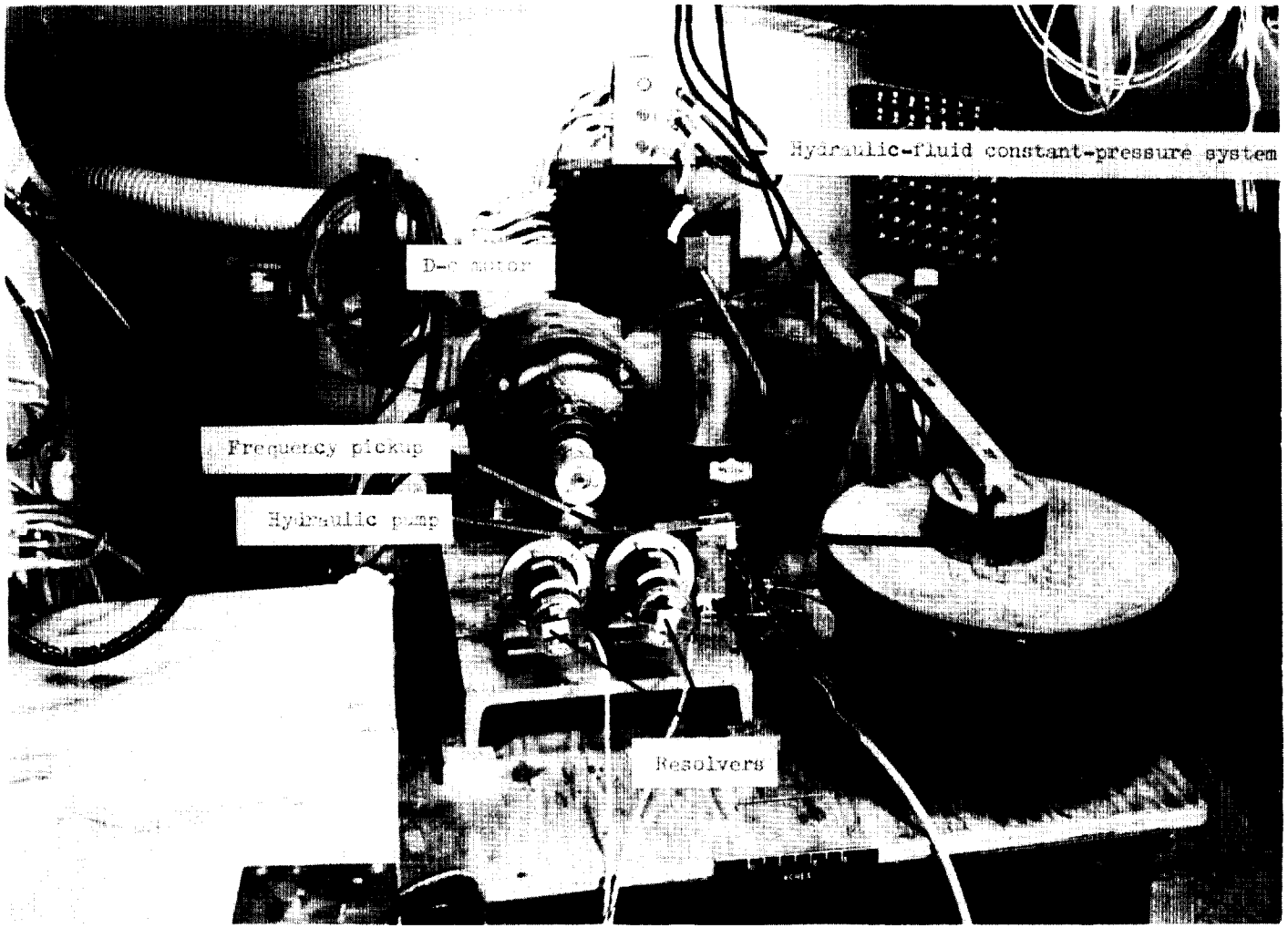

L-96053.1

Figure 4.- Externally mounted motor drive, hydraulic pump and components, and resolvers.

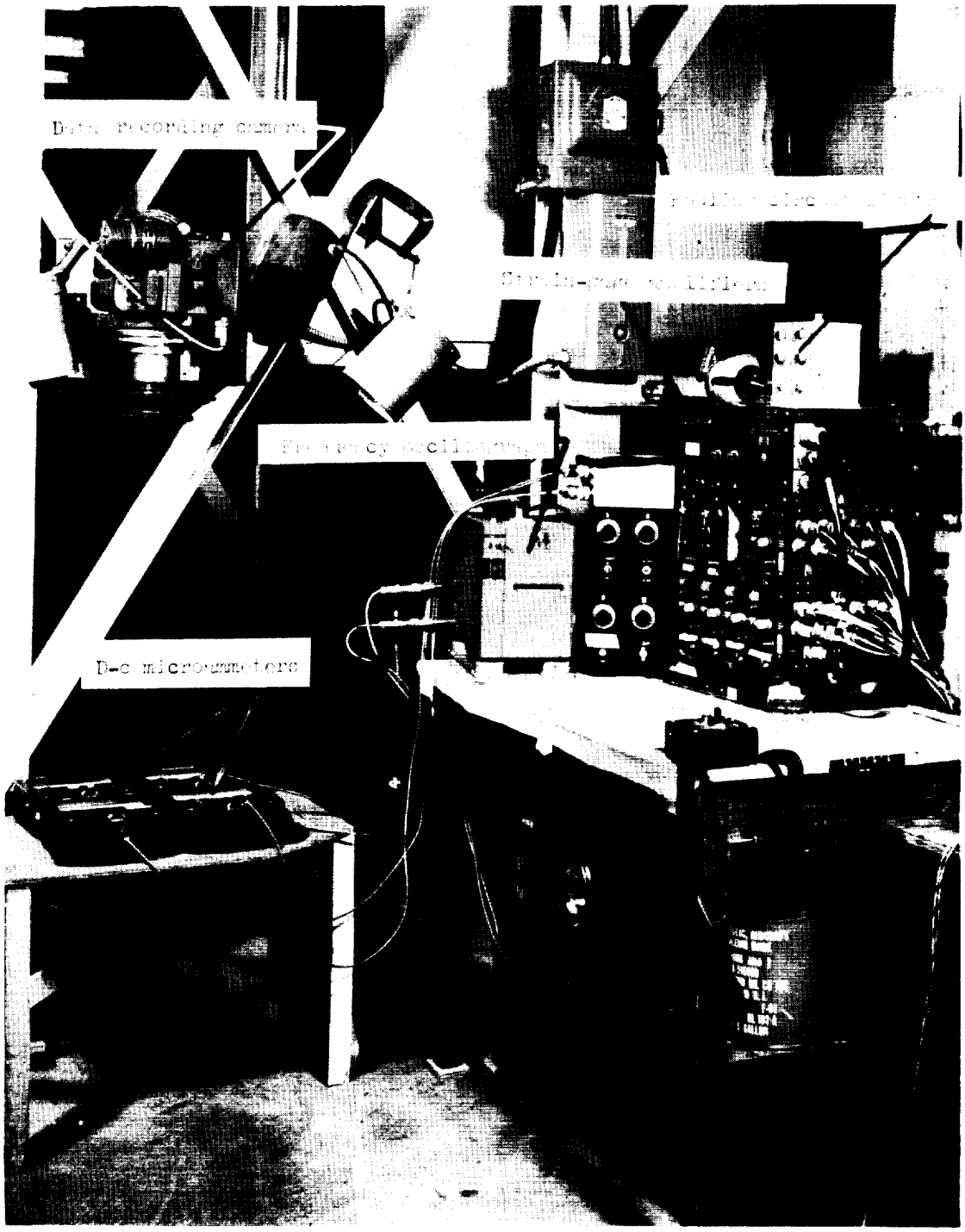

Figure 5.- Electrical instrumentation. L-96052.1

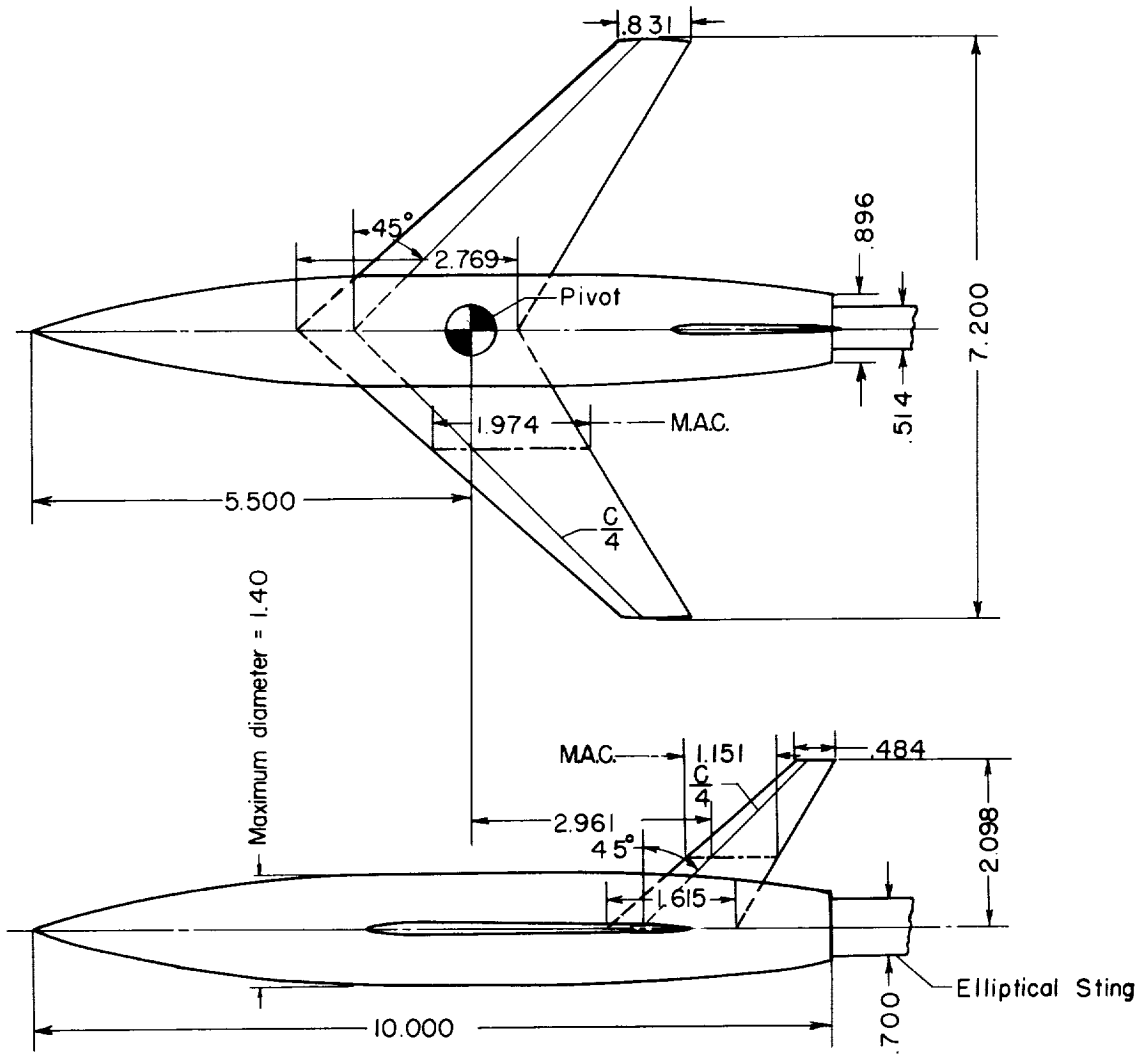

Figure 6.- Two-view drawing of model. (All dimensions in inches.)

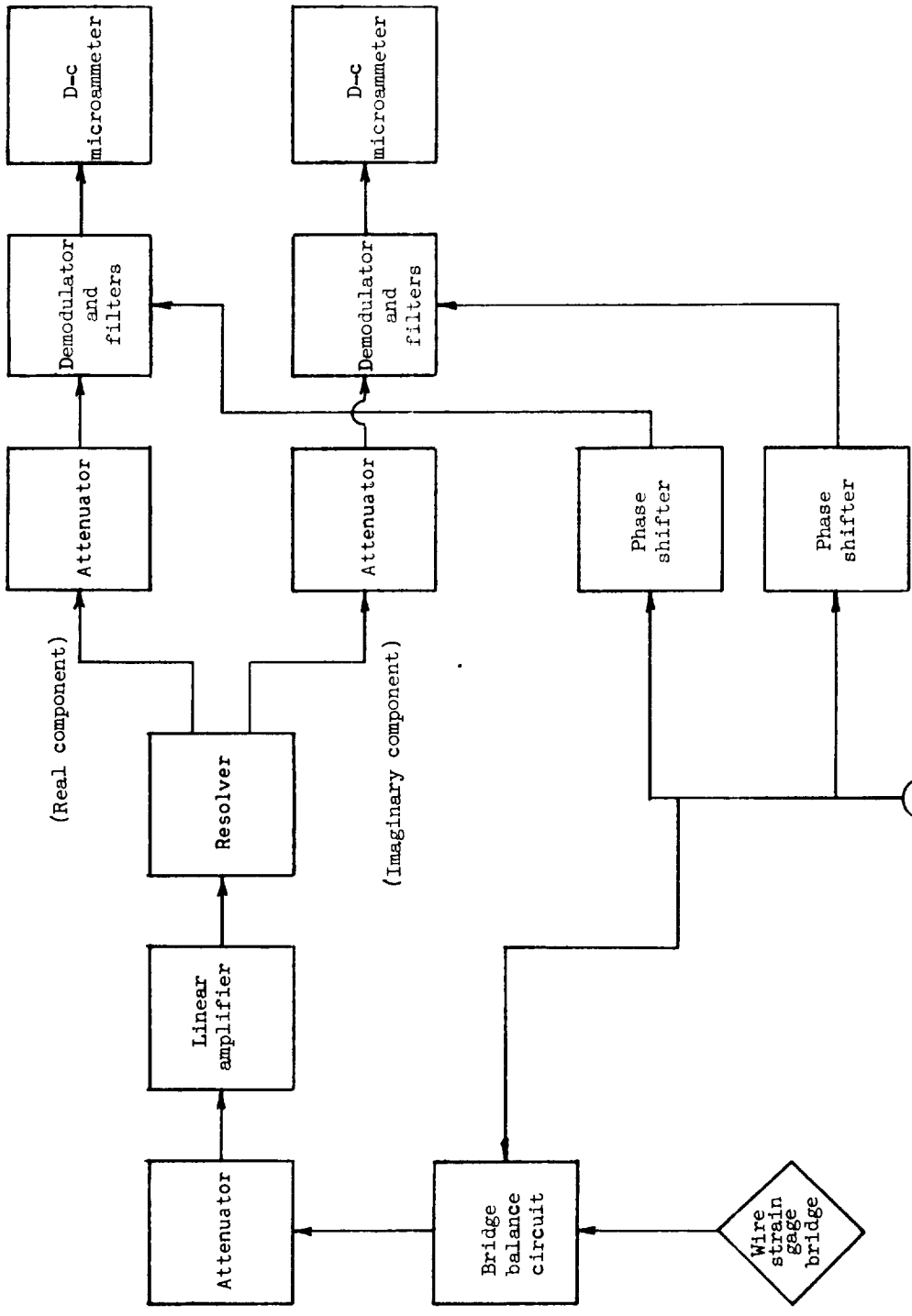

Figure 7.- Block diagram of electronic circuits used to measure model displacement and applied moment.

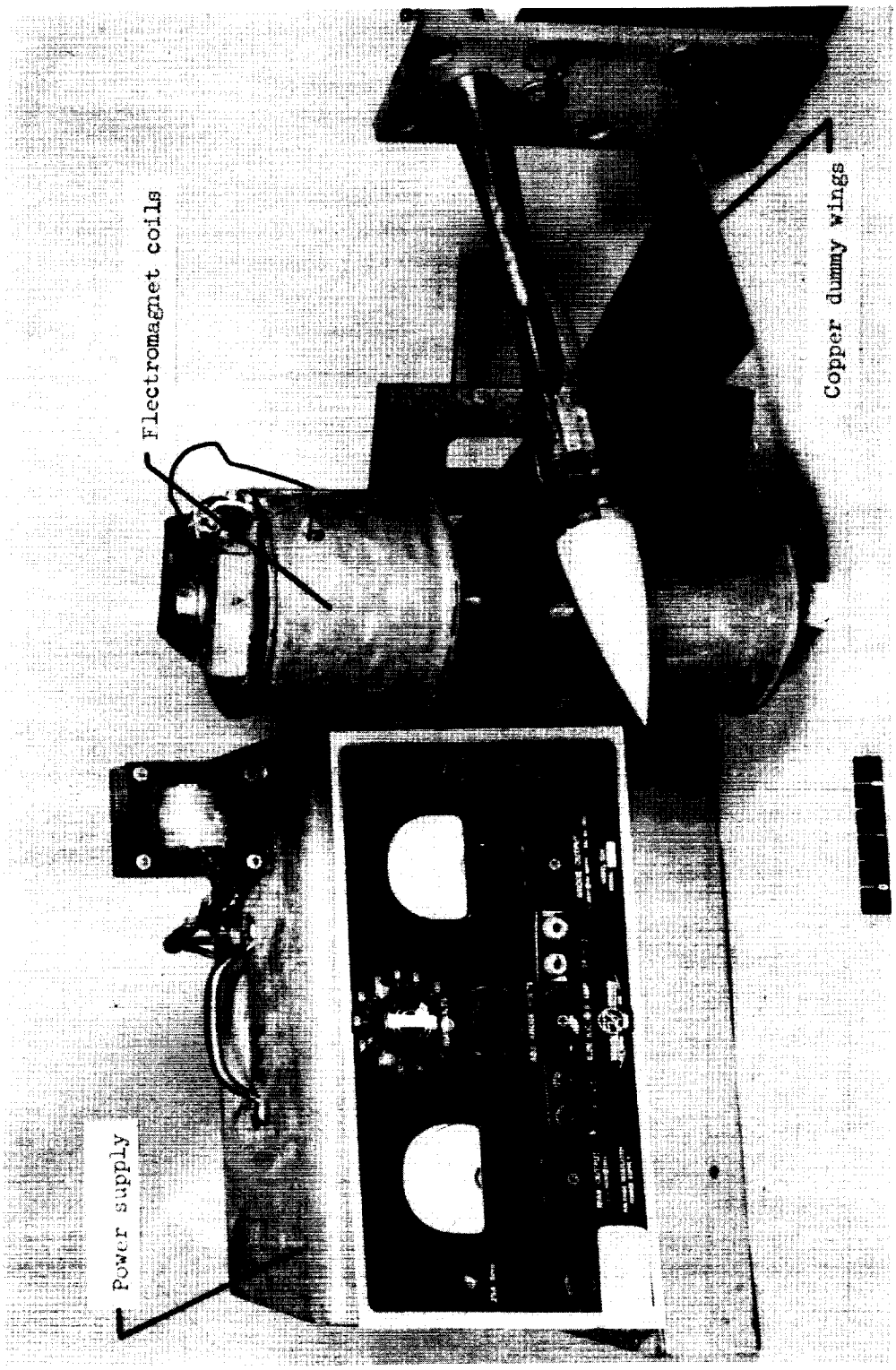

Figure 8.- Model with electromagnetic eddy-current damper installed. L-96638.1

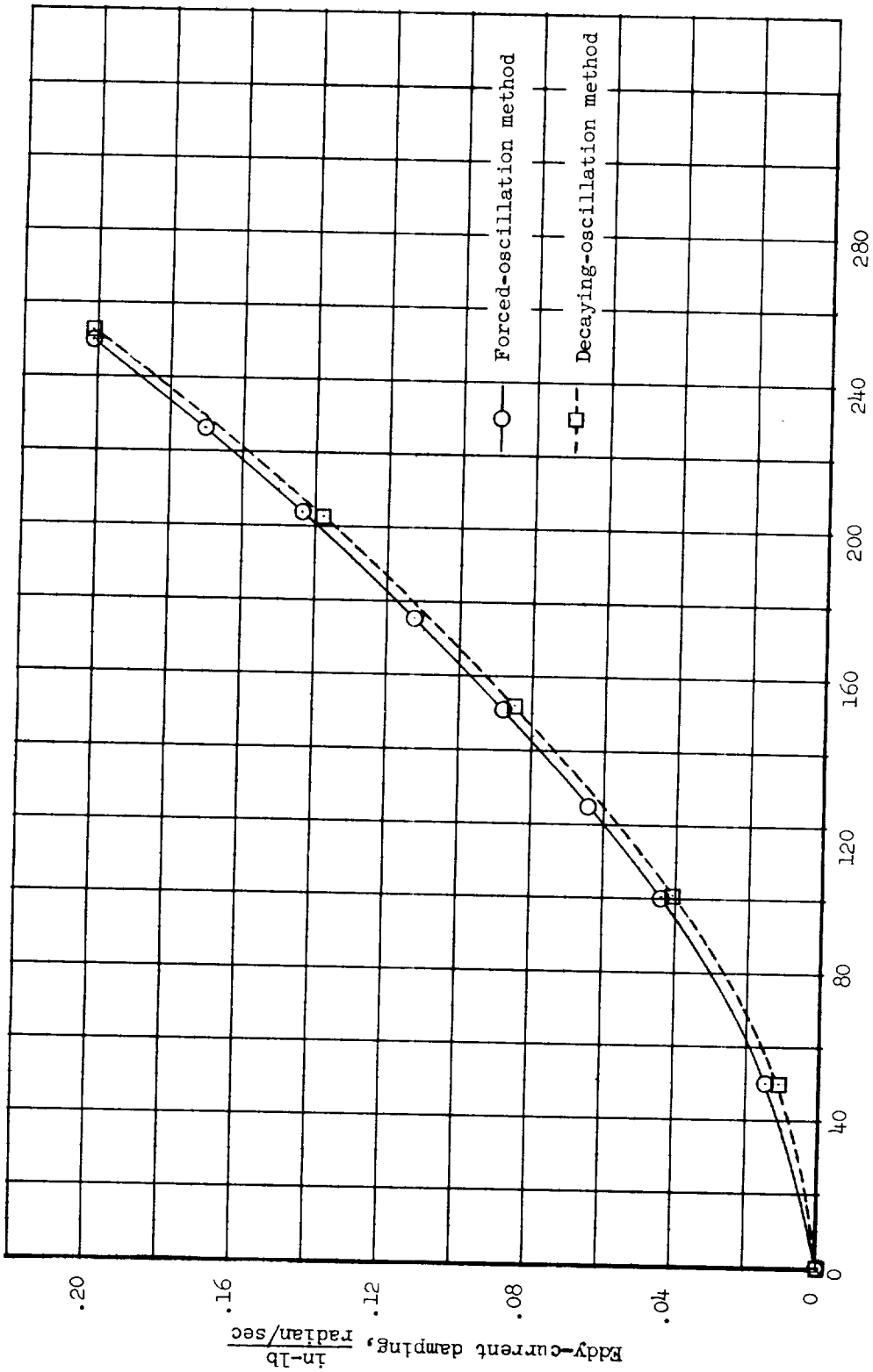

Figure 9.- Variation of measured eddy-current damping moment with damper coil current as determined by the free-decay and force-driven techniques.

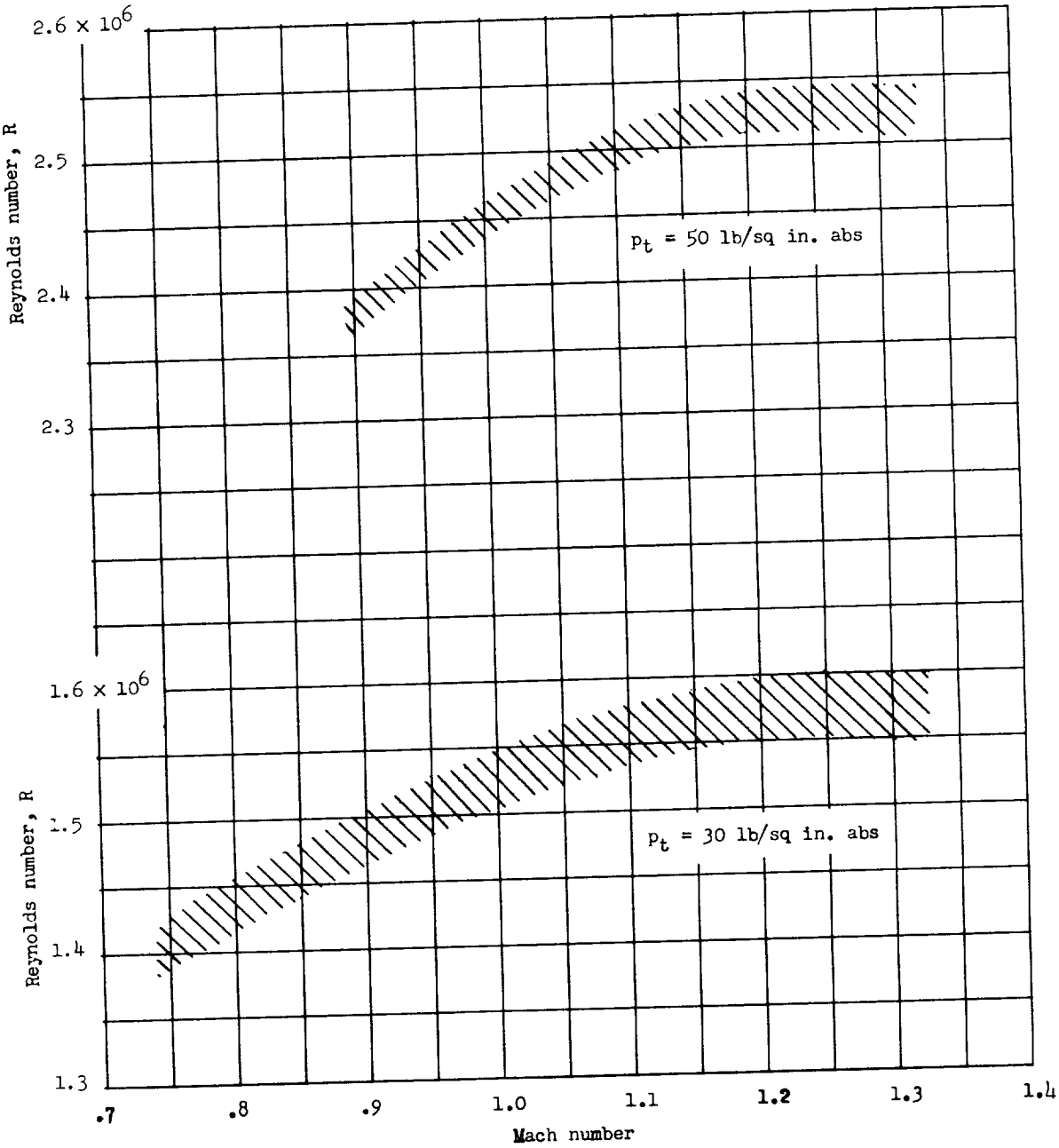

Figure 10.- Variations of Reynolds number with Mach number at constant wind-tunnel stagnation pressures.

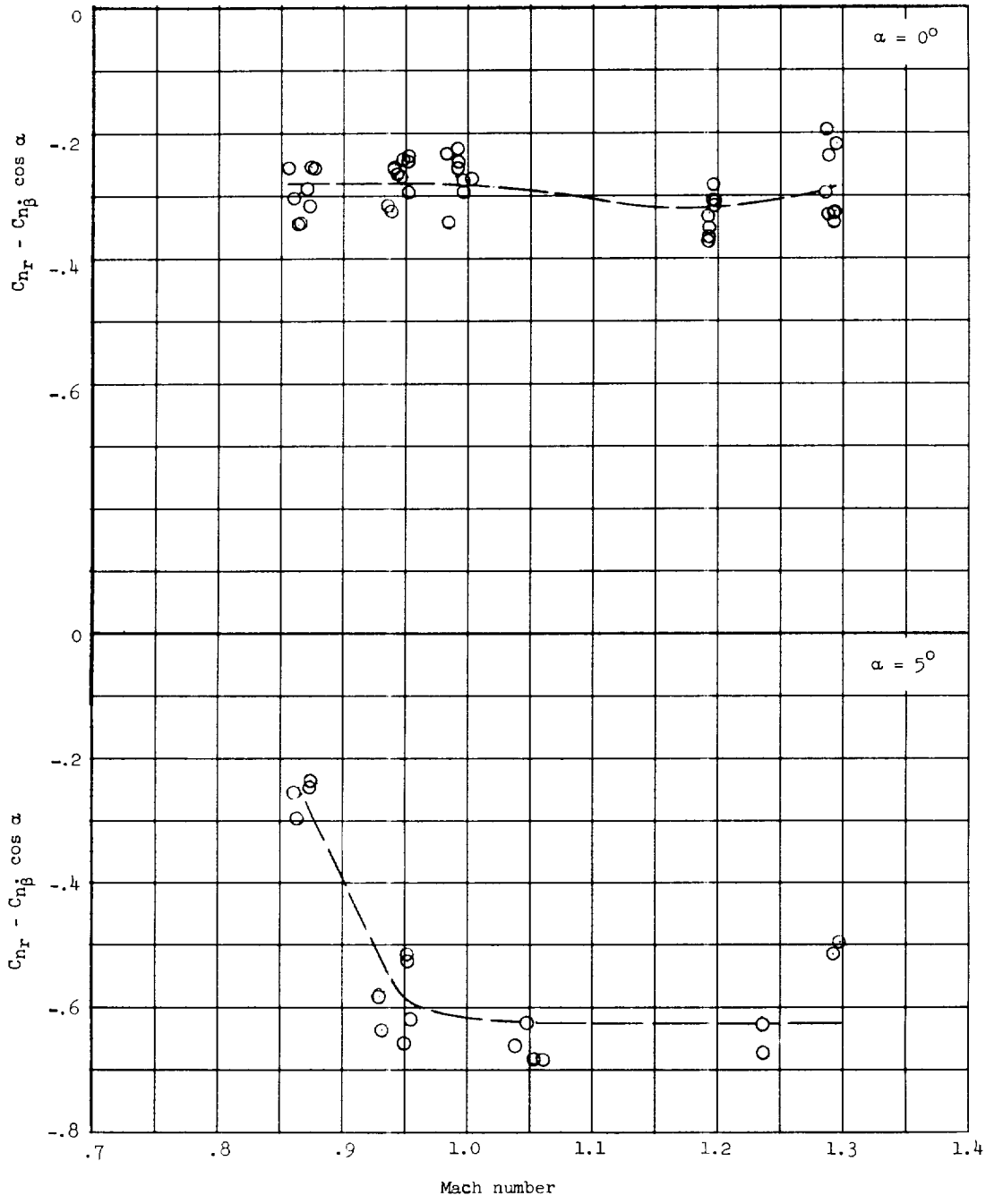

(a) Frequency spring 1; p_t = 30 lb/sq in. abs; $\omega b/2V$ = 0.038 to 0.057.

Figure 11.- Variation of the damping-in-yaw parameter $C_{n_r} - C_{n_{\dot{\beta}}} \cos \alpha$ with Mach number.

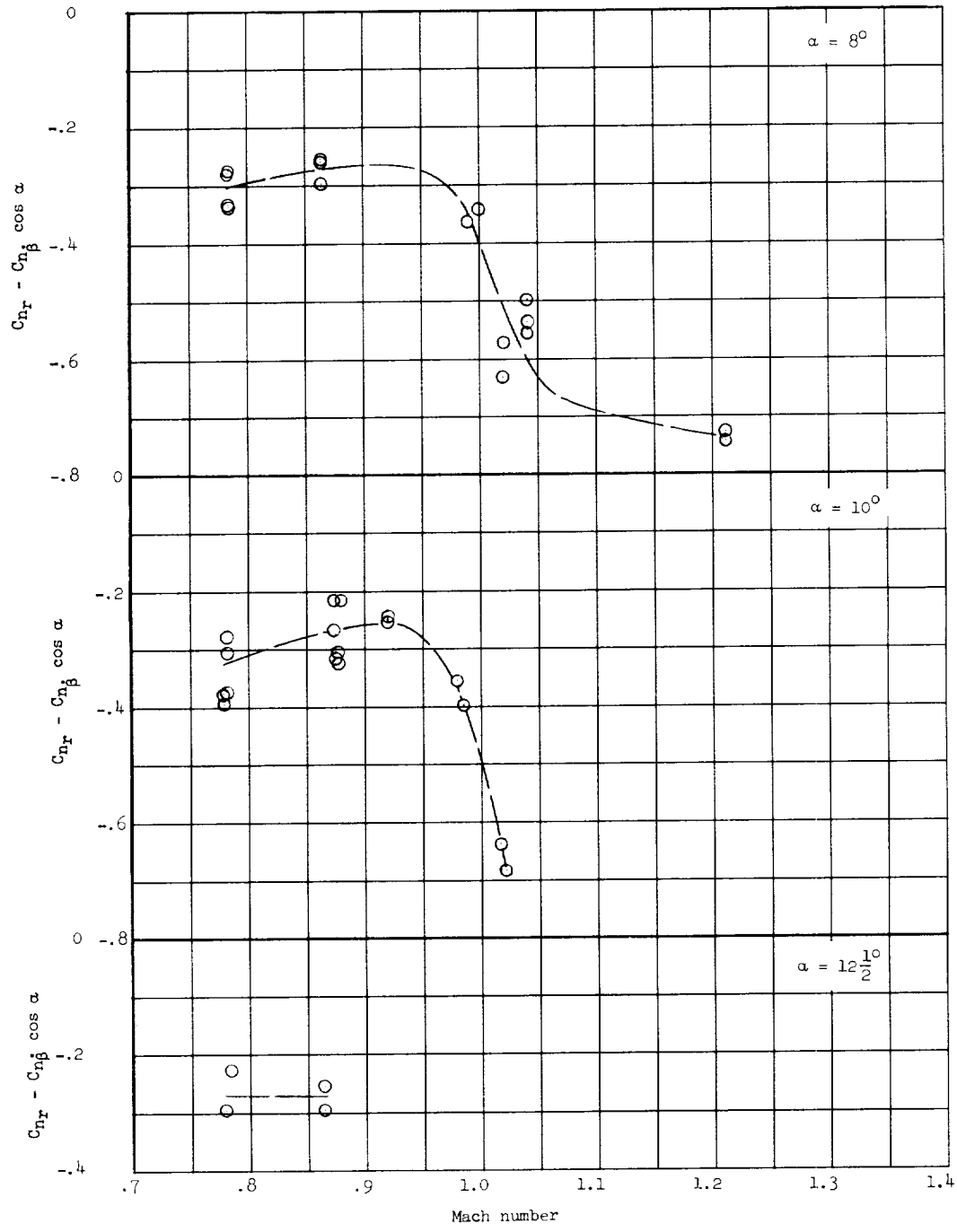

(a) Concluded.

Figure 11.- Continued.

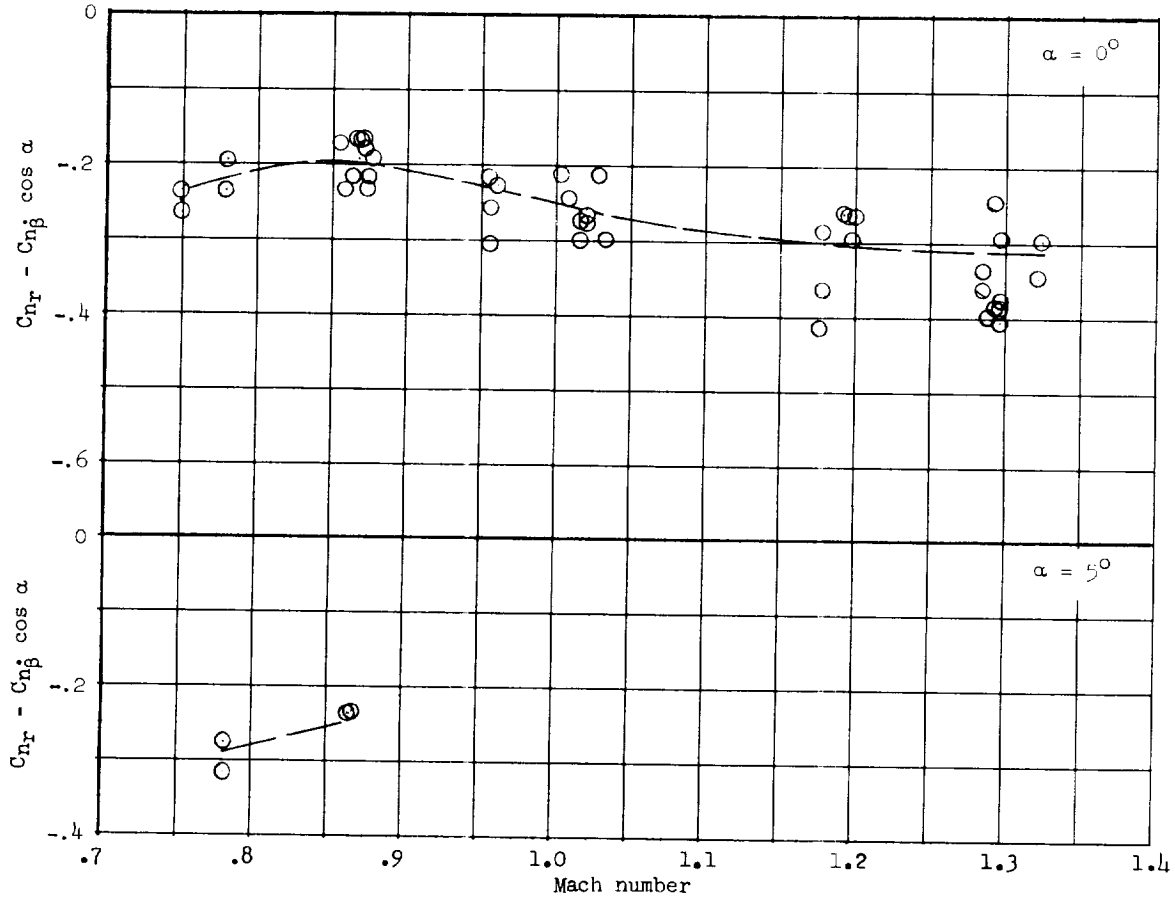

(b) Frequency spring 2; p_t = 30 lb/sq in. abs; $\omega b/2V$ = 0.034 to 0.049.

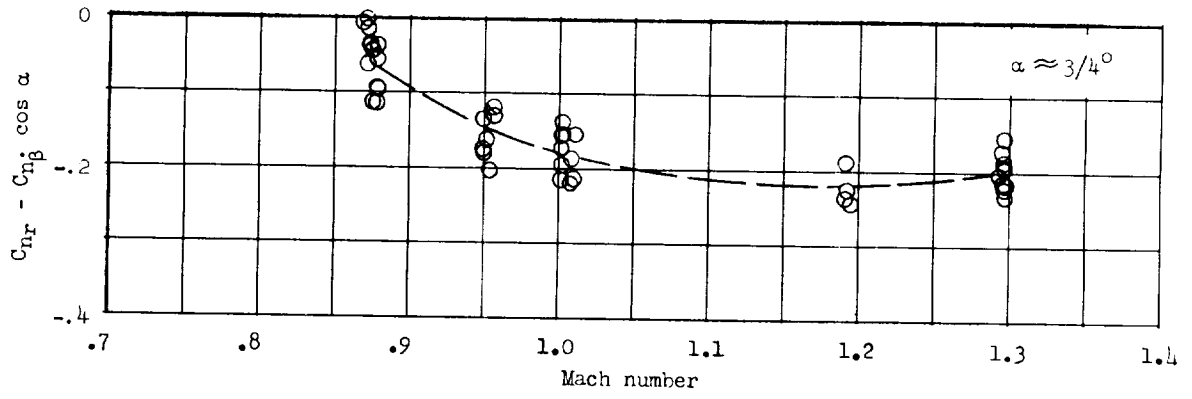

(c) Frequency spring 3; p_t = 30 lb/sq in. abs; $\omega b/2V$ = 0.030 to 0.039.

Figure 11.- Continued.

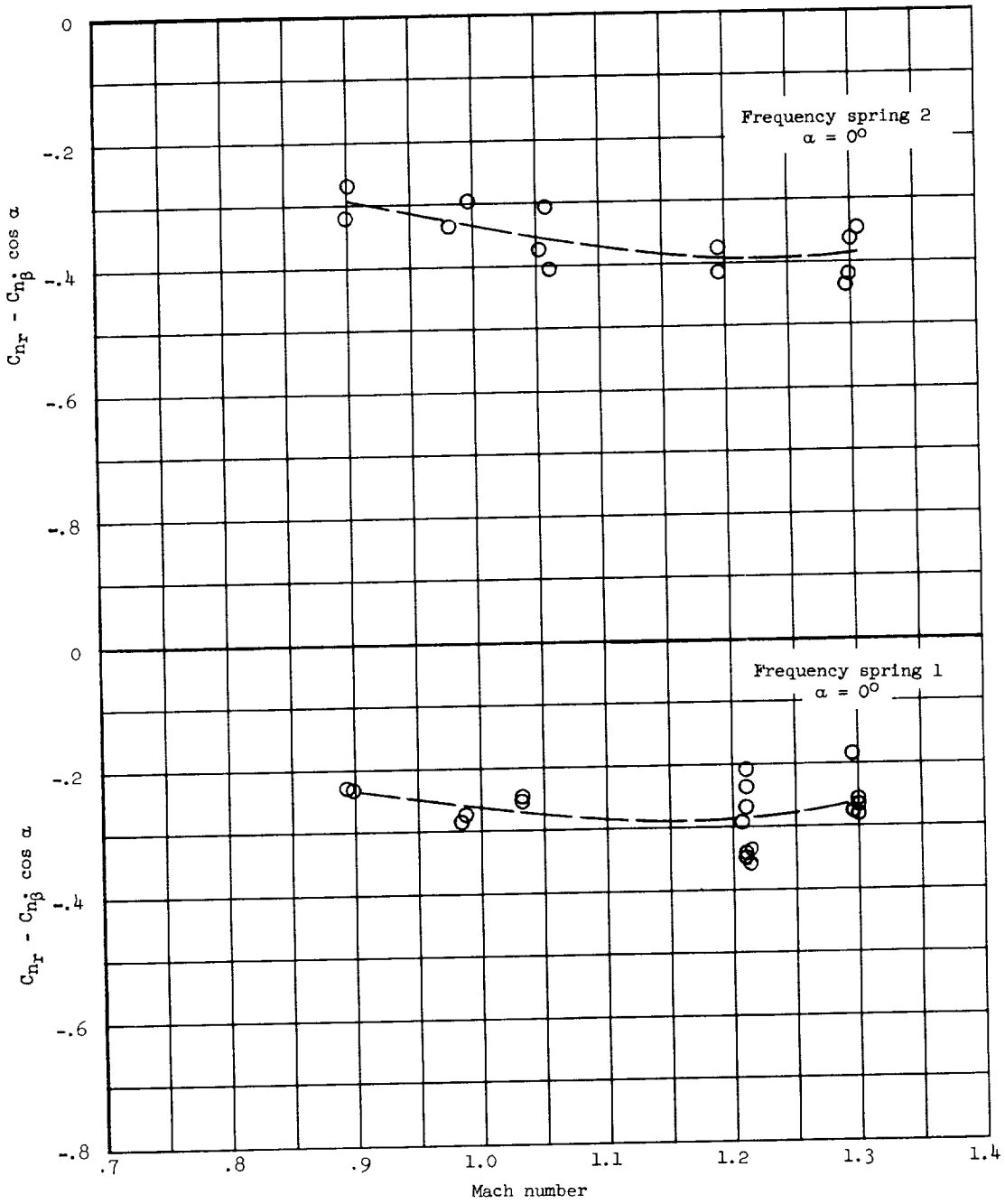

(d) Frequency springs 1 and 2; p_t = 50 lb/sq in. abs; $\omega b/2V$ = 0.037 to 0.051.

Figure 11.- Concluded.

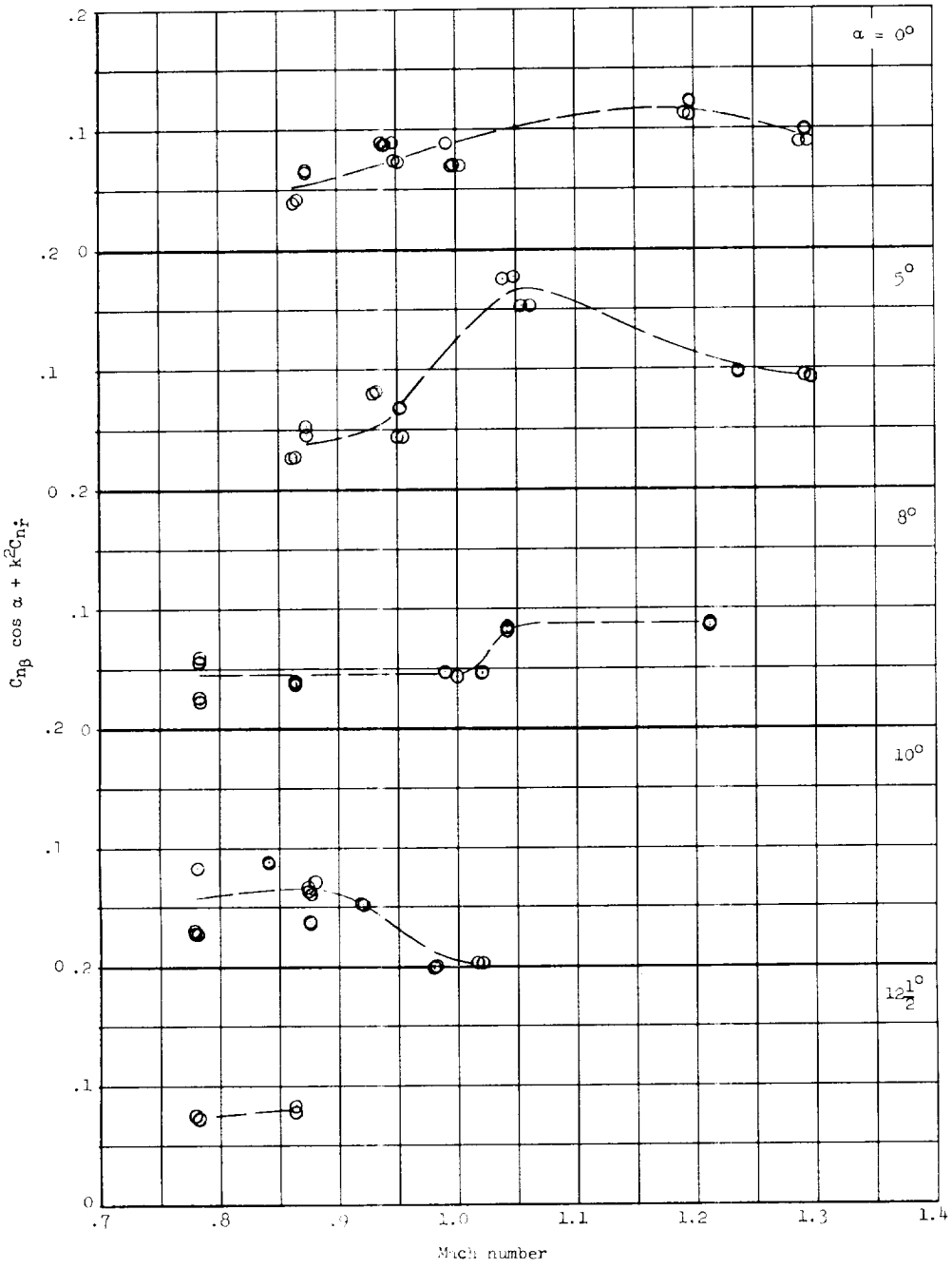

(a) Frequency spring 1; p_t = 30 lb/sq in. abs; $\omega b/2V$ = 0.038 to 0.057

Figure 12.- Variation of the oscillatory directional stability parameter $C_{n_\beta} \cos \alpha + k^2 C_{n_{\dot{r}}}$ with Mach number.

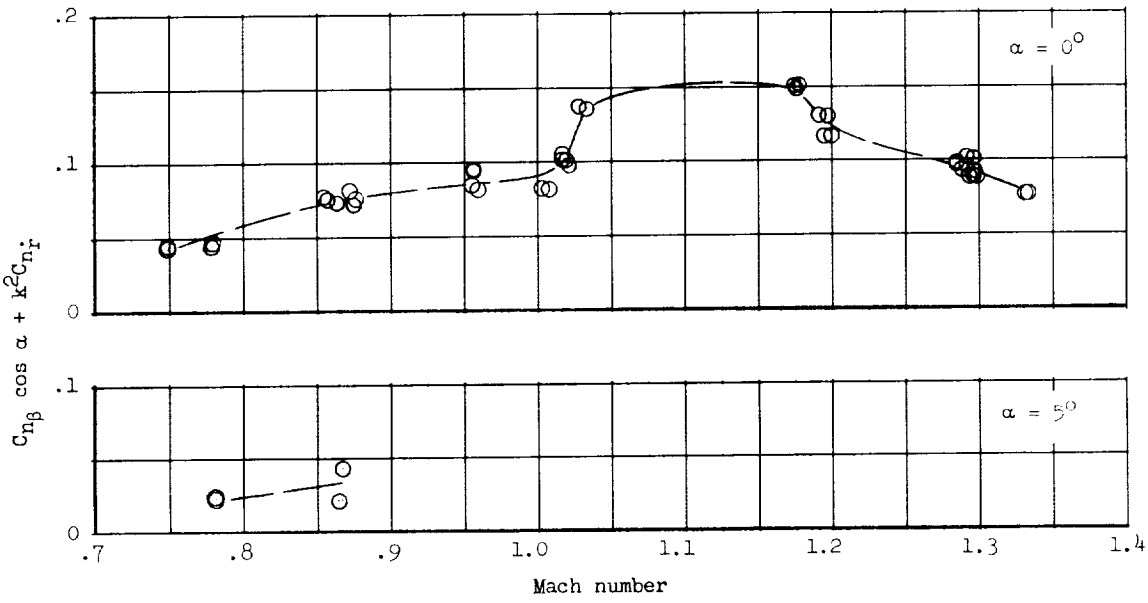

(b) Frequency spring 2; p_t = 30 lb/sq in. abs; $\omega b/2V$ = 0.034 to 0.049.

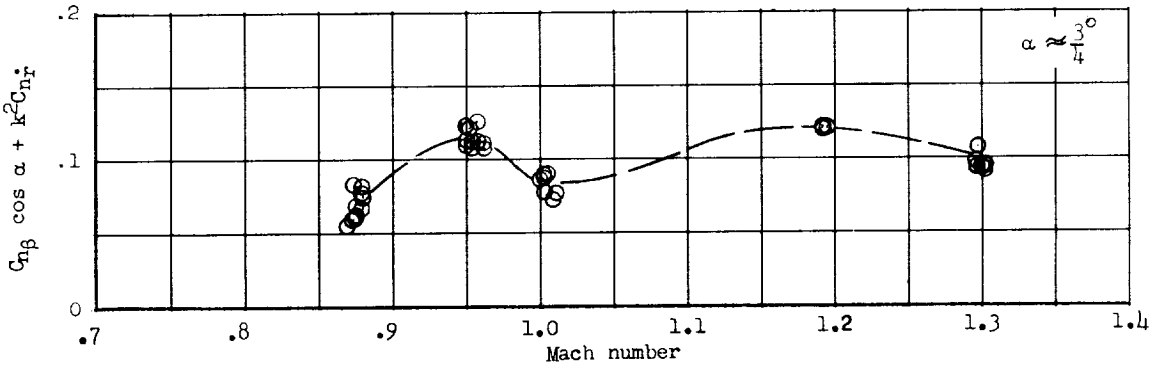

(c) Frequency spring 3; p_t = 30 lb/sq in. abs; $\omega b/2V$ = 0.030 to 0.039.

Figure 12.- Continued.

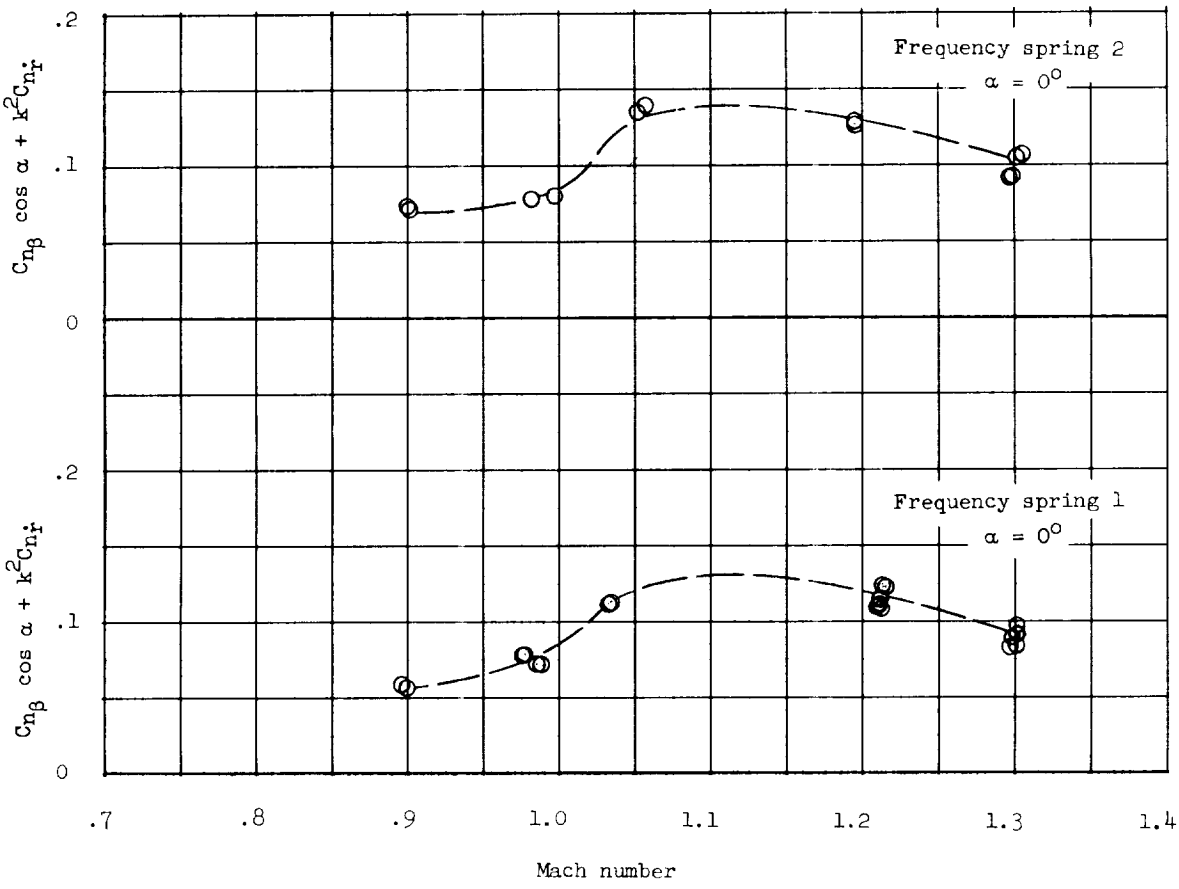

(d) Frequency springs 1 and 2; p_t = 50 lb/sq in. abs; $\omega b/2V$ = 0.037 to 0.051.

Figure 12.- Concluded.

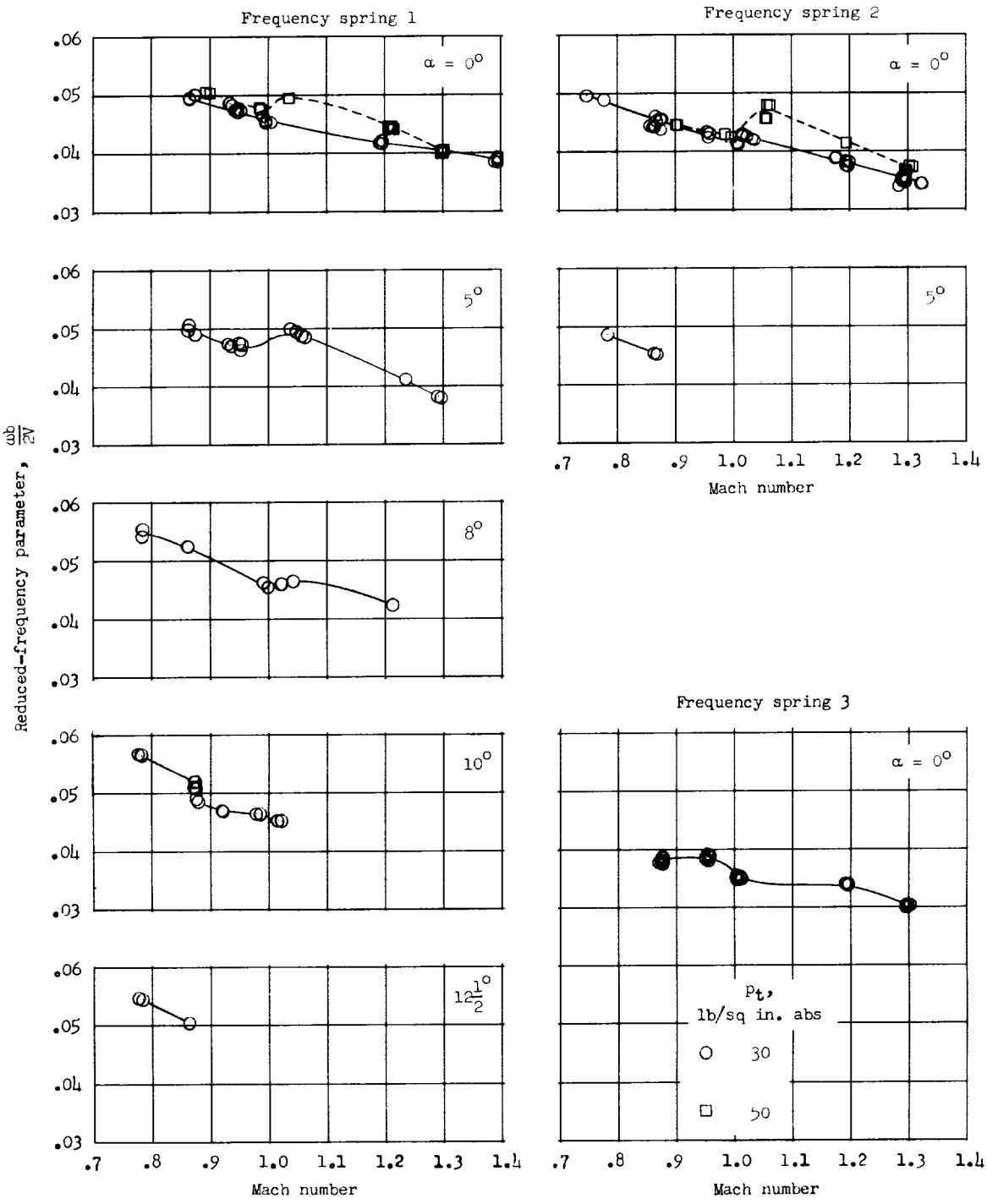

Figure 13.- Variation of the reduced-frequency parameter $\omega b/2V$ with Mach number for various test conditions.